J. Fluid Mech. (1966), *vol.* 26, *part* 4, *pp.* 651–687
Printed in Great Britain

Wind action on water standing in a laboratory channel

By G. M. HIDY
National Center for Atmospheric Research, Boulder, Colorado

AND E. J. PLATE
Fluid Dynamics and Diffusion Laboratory, Colorado State University, Fort Collins, Colorado

(Received 10 August 1965 and in revised form 6 January 1966)

The development of waves and currents resulting from the action of a steady wind on initially standing water has been investigated in a wind–water tunnel. The mean air flow near the water surface, the properties of wind waves, and the drift currents were measured as they evolved with increasing fetch, depth and mean wind speed. The results suggest how the stress on the water surface changes with an increasingly wavy surface, and, from a different viewpoint, how the drift current and the waves develop in relation to the friction velocity of the air. The amplitude spectra calculated for the wavy surface reflected certain features characteristic of an equilibrium configuration, especially in the higher frequencies. The observed equilibrium range in the high frequencies of the spectra fits the f^{-5} rule satisfactorily up to frequencies f of about 15 c/s. The wave spectra also revealed how the waves grow in the channel, both with time at a fixed point, and with distance from the leading edge of the water. These results are discussed in the light of recent theories for wave generation resulting from the action of pressure fluctuations in the air, and from shearing flow instabilities near the wavy surface. The experimental observations agree reasonably well with the predictions of the recent theory proposed by Miles, using growth rates calculated for the mechanism suggesting energy transfer to the water through the viscous layer in the air near the water surface.

1. Introduction

When turbulent air passes over water initially standing in a channel, small surface waves are generated and a drift current develops in the water. As the waves grow with fetch and duration of air motion, the aerodynamic roughness of the water surface changes, causing modification in the vertical profile of the mean air flow above the water surface. Energy is transferred from the air motion to the water and is partitioned between the drift current and the surface waves. The wind waves in turn alter the air velocity distribution. Thus, a complex mechanism of air–water interaction and feedback takes place which as yet is not fully understood in all its details.

Although there exists a large body of theoretical information dealing with various idealized models of air–water interaction, relatively few laboratory

studies treating this subject are available. As Ursell (1956) has noted, new experimental investigations carried out under controlled conditions are essential to further progress in this field. This paper is intended to contribute towards filling the gap between theory and experiment by reporting some new measurements of combined air and water motion in a laboratory channel. Several interesting features of these results are discussed in the light of previous laboratory investigations, and of recent theoretical developments.

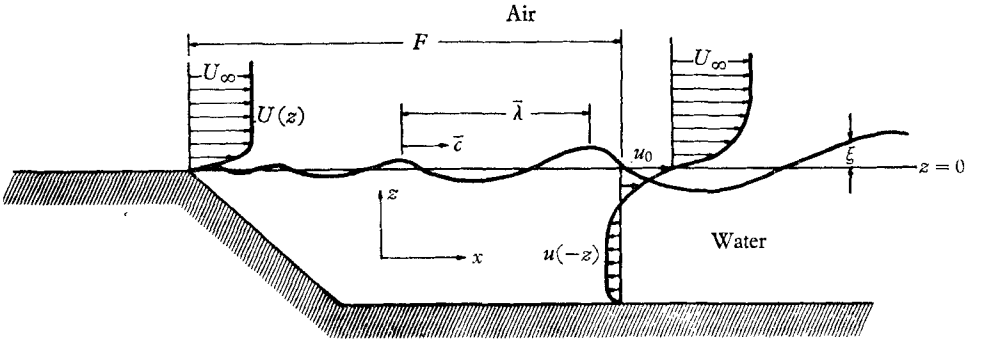

FIGURE 1. A schematic drawing of air and water motion associated with growing waves on a water surface.

To describe the air and water flow as it develops in the closed rectangular channel, a scheme of reference will be used as sketched in figure 1. The co-ordinate system is indicated such that x is the distance downstream, and z is the vertical direction. The mean water surface is given by $z = 0$ while the surface displacement from this level is denoted as ξ. The fetch F represents the distance from the leading edge of the water to a particular point somewhere downstream. A two-dimensional model for the fluid motion is assumed, with the velocity in the water given by $u(-z)$, and the drift at the water surface denoted as u_0. The air velocity is given by $U(z)$, and U_∞ denotes the air velocity at approximately 20 cm above the mean water surface. The wavelength $\bar{\lambda}$, and the phase speed $\bar{c}$ represent the properties of significant waves. For the purposes of this study, the significant waves will refer to the larger, regular waves observed at a given fetch. In general, smaller ripples are superimposed on the larger disturbances (see, for example, figure 2 (plate 1)).

2. Experimental equipment and procedure

The experiments were conducted in the wind–water tunnel at Colorado State University. This facility has been described in detail by Plate (1965). Briefly, it consists of a smooth-bottomed wind tunnel 0·61 m wide by 0·76 m high whose Plexiglass test section has a length of about 12 m. The channel was hydraulically smooth everywhere. An axial fan controlled the air discharge through the tunnel. The air motion was made uniform by fine mesh screens and honeycombs at the inlet converging section and just upstream of the outlet diffuser. During operation, water can stand in the tunnel up to depths of 15 cm. Sloping beaches of aluminium honeycomb prevent reflexion of waves at the inlet and outlet. The

inclined beaches also are shaped in such a way that a smooth transition takes place between the adjoining air and water flow.

The air speed in the tunnel was measured by a Pitot–static tube in conjunction with an electronic micromanometer. The probe was placed on a carrier which could be positioned anywhere in a given section of the tunnel from the bottom to a level about 10 cm from the top.

Pressure gradients in the air, and the depth of the water were measured every 1·2 m down the tunnel with piezometer taps connected to a set of manometers, consisting of glass tubes.

Phase speeds and lengths of significant waves were determined from movies. The lengths for successive waves were obtained from the films by measuring the distance between crests with a ruler located in the picture. The phase velocities of waves referred to a fixed point were estimated by measuring from adjacent frames the distance travelled by a given crest during the time between successive frames. The time intervals between frames were read from a timer that was shown on the film.

Capacitance probes were installed every 1·2 m along the centreline of the tunnel to measure the water surface displacement as a function of time. The probes consisted of 34-gauge magnet wires which were stretched vertically across the tunnel perpendicular to the water surface. The copper wires and the water formed two plates of a condenser, and the wire insulation (Nyclad) provided the dielectric medium. The wires were calibrated before each series of experiments. The capacitance between the wire and the water was measured with an a.c. excited bridge; the unbalance voltage from the bridge was linearized, amplified, and rectified so that a d.c. output voltage was obtained which was proportional to the water depth. The output signal was fed to an oscillograph recorder. The capacitance bridge–oscillograph combination was calibrated to give a recorded amplitude linearly proportional to the (varying) water depth with a flat response to frequency ($\pm 1\%$) up to approximately 30 cyc/sec.

It was not possible to obtain the vertical velocity distribution in the water. However, the surface velocity of the water was estimated roughly by placing a small 2 mm diameter buoyant particle on the water and measuring the time required for it to move past fixed stations downstream.

In this study, attention was centred on the measurement of the properties of water waves under conditions of steady (mean) air motion. In order to attain steady conditions in the air flow, in the wave development, and in the set-up of water in the tunnel, the fan was started about 15–20 min before the properties of the fluid flow were to be measured. After this time interval, the photographs, the Pitot tube measurements, and the wave-amplitude data were taken, and a sample of wave train corresponding to the passage of 100 or more significant waves was recorded for a given run.

Observations of wave development were made for several different conditions. For water initially standing in the horizontal channel, air velocities, taken 20 cm above the water surface, were varied from 0 to 15 m/sec while the depth of water was changed from 2·5 to 10 cm. The properties of fluid motion under conditions of steady flow were observed at fetches of approximately 1·8 to 12 m.

Some measurements also were made of the transient wave pattern that developed at a given point when air, in analogy to a step input, was suddenly passed over a still, smooth water surface. The data for dynamic air pressure in these experiments showed that the time required to build up a steady air velocity was short compared with the time to raise waves. During these runs, a steady wave pattern was signalled by the observation that the amplitude of significant waves displayed no further increase with time. This state was checked by observing whether or not the wave spectra became the same for successive sections of the oscillograph recordings of surface displacement.

The detailed structure of the local air motion could not be measured for the transient runs; therefore, the distribution of air velocity for these experiments was assumed to be the same as that corresponding to the limit of the steady-flow conditions.

From the continuous records of surface displacement, data were digitized at equal time intervals of 0·0125 or 0·025 sec. These data were used for obtaining values of the standard deviation σ, the autocorrelation function, and the spectral-density function of the surface displacements. The statistical computations were made on a digital computer following the methods discussed by Blackman & Tukey (1958).

For conditions of steady flow, good samples of the water surface displacement were collected by taking recordings which were long enough to ensure a reliable statistical sampling of the largest waves. However, in the transient experiments, this could not be done. Since the waves grew rapidly after the onset of wind action, only very short samples of 20 sec length could be recorded for the transient cases. The oscillograph records for these experiments had to be cut into pieces, and the mean value of the water surface for each piece had to be subtracted out to obtain approximately quasi-steady samples. The pieces of record contained at least twenty significant waves, but this probably is not enough to ensure completely reliable statistical samples.

3. Results

3.1. *Air flow over the water*

Since the air is forced by the fan through the wind tunnel of approximately constant cross-section, a pressure gradient develops in the downstream direction. The pressure gradient increased with wind speed and with depth of the water. For given conditions of air flow and depth, the pressure gradient remained approximately constant over the last 6 m of the tunnel. The average value of the pressure gradient in this region was used for all subsequent calculations. The complete set of data for the pressure gradients has been presented by Plate & Goodwin (1965), and some examples have been given by Hidy & Plate (1965*a*).

The mean horizontal air speeds in the vertical direction and across the channel were measured at several sections for air speed of U_∞ from 6 m/s to about 14 m/s. Typical vertical profiles along the centre section of the channel are shown in figure 3 (*a*). They indicate that the air flow generally develops a behaviour characteristic of turbulent flow in a boundary layer over roughened surfaces.

Typical measurements of the horizontal distribution of velocity are shown in figure 3(*b*). These data are representative of flow in wind tunnels of rectangular cross-section, and display rather thick boundary layers on the side walls. The three-dimensional field of velocity in the air was not reflected, however, in the geometry of significant waves in the channel. As shown in figure 2 (plate 1), the waves still exhibited nearly linear crests moving approximately normal to the mean wind direction.

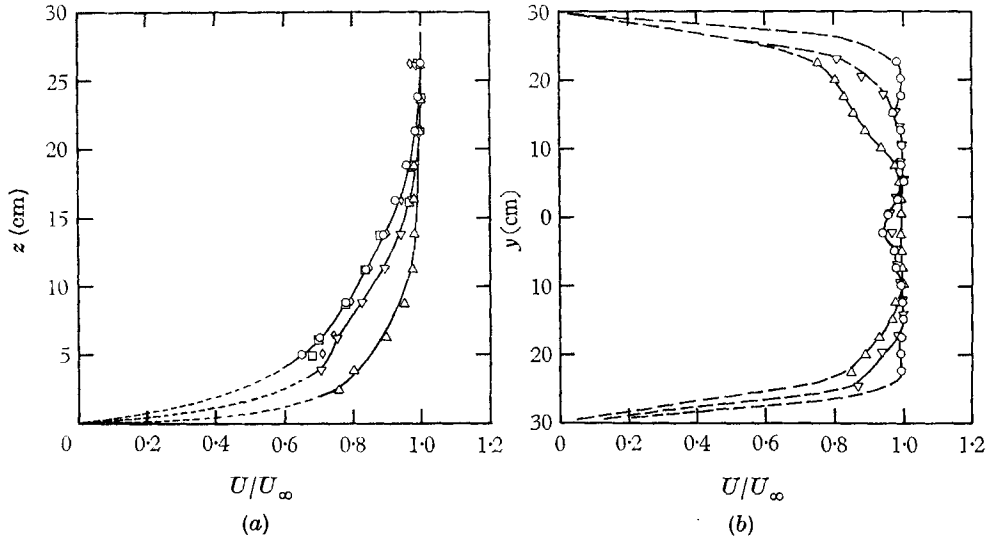

FIGURE 3. Typical distributions of air flow in the wind–water tunnel. (*a*) Vertical profiles taken along the centre section. (*b*) Horizontal profiles taken at $z \approx 20$ cm.

	(*a*)			(*b*)	
	F(m)	U_∞(m/sec)		F (m)	U_∞(m/sec)
△	2·14	10·8	○	2·14	10·8
▽	4·58	12·2	▽	7·11	12·9
□	7·11	12·9	△	11·9	14·5
◇	9·43	13·4			
○	11·9	14·5			

Since the three-dimensional structure of the air flow does not visibly affect the waves generated on the water surface, or the horizontal distribution of drift near the water surface, the motion of the air and the water generally will be treated as two-dimensional as illustrated in figure 1. That is, only a narrow, 'uniform' region of fluid flow near the centre of the channel will be considered.

3.2. *Properties of the wind-induced water motion*

Even though the air speed U_∞ reached values exceeding 14 m/sec, only small gravity waves and capillary ripples developed on the water surface. Breaking of waves, in the sense of forming white caps, was not observed. At high air velocities droplets of spray were observed being shed from crests of the larger waves, but the waves did not become sharp crested as seen in 'fully developed' seas.

Up to wind speeds U_∞ of about 3 m/sec, no waves appeared on the water surface. However, very small oscillations of the entire water surface could be observed in this range of air flow by watching variations in reflected light on the water. When the (steady) wind speed U_∞ exceeded 3 m/sec, initial ripples developed on the water surface closer to the leading edge of the water the higher the wind speed. The small disturbances that initially made an appearance on the water had wavelengths of 1–3 cm. Although the water surface containing these wavelets had a three-dimensional mottled character, the direction of propagation of wavelets tended to be oriented in such a way that the crests were normal to the wind direction. As the wind speed increased, and the fetch increased, the ripples became larger in amplitude and length. Under the action of steady air motion, the waves travelled downstream at an increasing speed, while growing both in amplitude and in length. For wind speeds in the range U_∞ = 3–6 m/sec, significant waves developed from the initial ripples, and travelled with crests approximately normal to the wind direction, with smooth windward surfaces, and rippled leeward surfaces. Above U_∞ about 6 m/sec, capillary ripples were noted on both the windward and the leeward sides of the significant waves. At any given point downstream from the inlet, groups of 5–20 small gravity waves of nearly the same period passed by. These groups were separated by relatively calm regions of short duration, with small ripples having varied periods. The existence of groups of waves separated by relatively calm water suggests that there is an interference between different components of the wave train giving an appearance of 'beats'.

Typical examples of the development of waves with wind speed are shown in figure 2 (plate 1). These observations were taken at a fetch of about 8 m. Smaller ripples on the larger regular waves are observed at higher wind speeds. In addition there seems to be a tendency for larger waves to be slightly steeper in slope on the leeward side than on the windward side.

Typical magnitudes of the observed wavelengths and phase speeds for significant waves generated at $U_\infty \approx 6$ m/sec were 10 cm and 40 cm/s. Since the phase speeds were much smaller than the wind speeds, the waves generated under our laboratory conditions, as shown later, were closely related to the motion of the air in the layers nearest the water surface. The portion of the boundary layer in the air nearest the water follows the 'law of the wall' as indicated in figure 11. Thus, the distribution of air velocity depends on the aerodynamic roughness of the surface, and on the friction velocity U^*, defined in the usual way. The velocity of the centre part of the air flow U_∞ therefore has relatively little direct significance for air–water interaction under our experimental conditions. Hence, the parameter of air velocity used in the following discussion for the effect of wind on the waves is chosen as U^*.

The development of waves and currents. The growth of waves with fetch, with depth, and with wind speed is reflected in two characteristic lengths, the standard deviation σ, and the wavelength $\bar{\lambda}$ as shown in figure 4. A decrease in depth tended to reduce the wavelength and the standard deviation of the waves generated at higher wind speeds (higher friction velocities).

Two characteristic velocities associated with the water motion are the surface

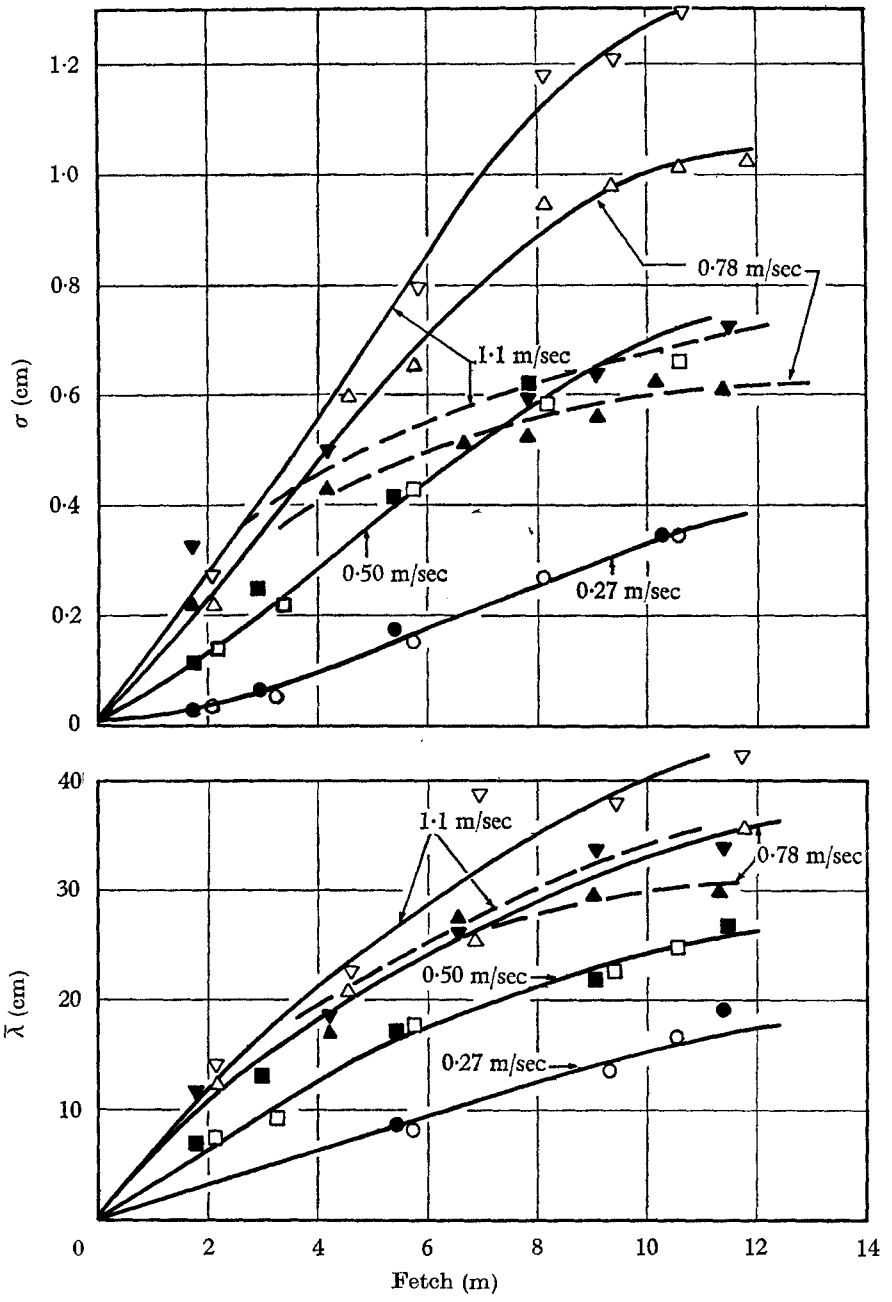

FIGURE 4. Variation in characteristic lengths of surface waves with mean friction velocity fetch, and water depth.

	U^* (m/sec)	d (cm)		U^* (m/sec)	d (cm)
○	0·27	10·2	●	0·27	5·1
□	0·50	10·2	■	0·50	5·1
△	0·78	10·2	▲	0·78	5·1
▽	1·1	10·2	▼	1·1	5·1

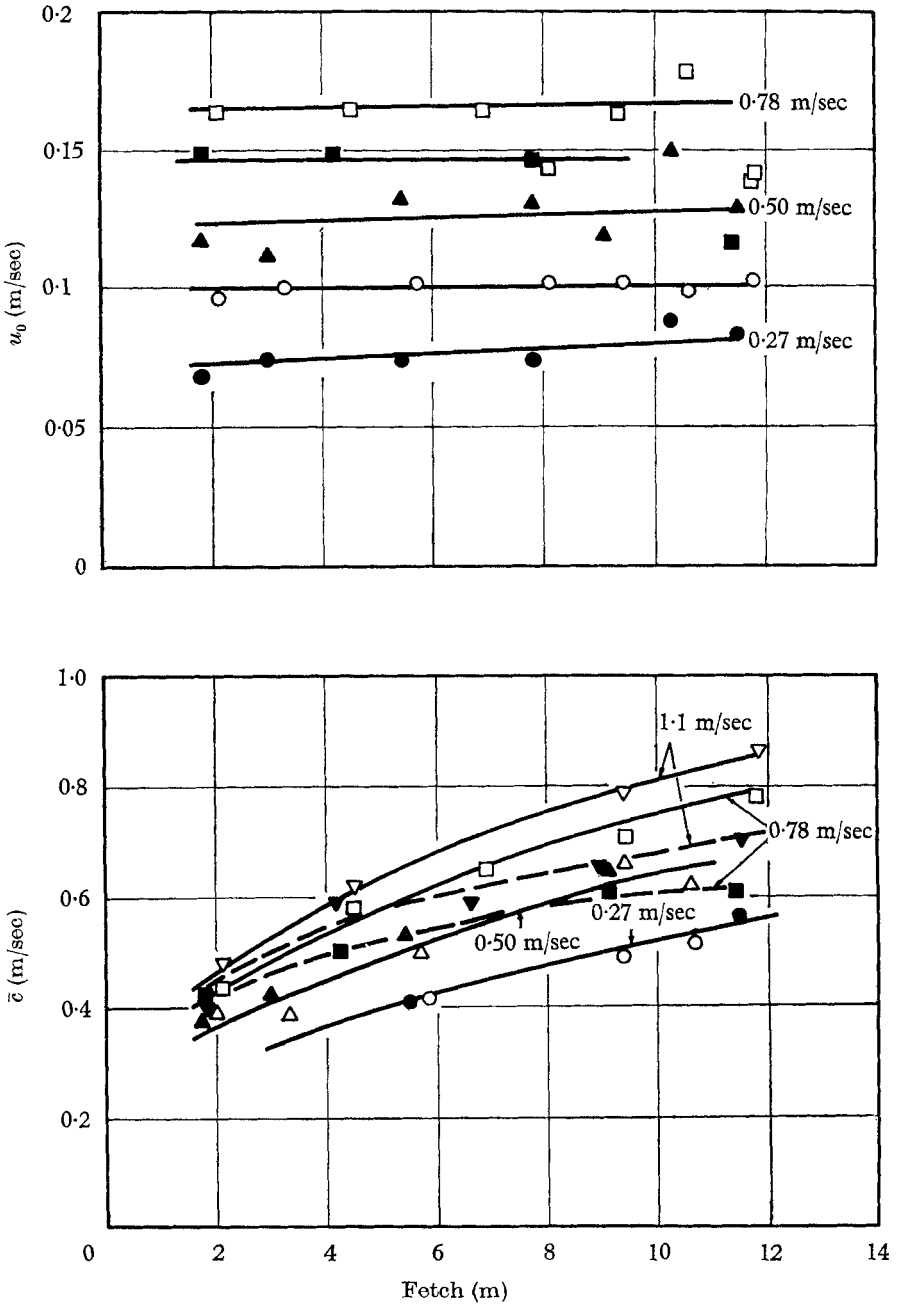

FIGURE 5. Variation in characteristic water velocities with mean friction velocity, fetch, and depth.

	U^* (m/sec)	d (cm)		U^* (m/sec)	d (cm)
○	0·27	10·2	●	0·27	5·1
△	0·50	10·2	▲	0·50	5·1
□	0·78	10·2	■	0·78	5·1
▽	1·1	10·2	▼	1·1	5·1

velocity u_0, and the phase speed of significant waves, $\bar{c}$. The change with fetch, friction velocity, and depth of these properties is shown in figure 5. For a given wind speed, the surface drift tends to increase slightly with increasing fetch over the range of depth shown, except near the ends of the channel. The measured phase speed is approximately independent of depth down to 5·1 cm for U^* up to 0·63 m/sec. However, at higher values of U^*, the water depth begins to affect $\bar{c}$. The values of $\bar{c}$ generally increase with increasing friction velocity and fetch.

Autocorrelation functions and frequency spectra. The time correlations between displacements of the water surface were calculated from the digitized oscillograph records. The autocorrelation function $R(\tau)$ is defined as

$$R(\tau) = \overline{\xi(t_1)\,\xi(t_2)}, \quad \tau = (t_2 - t_1), \tag{1}$$

where $\xi(t_1)$ and $\xi(t_2)$ are surface displacements taken at the same point for two different times, t_1 and t_2.

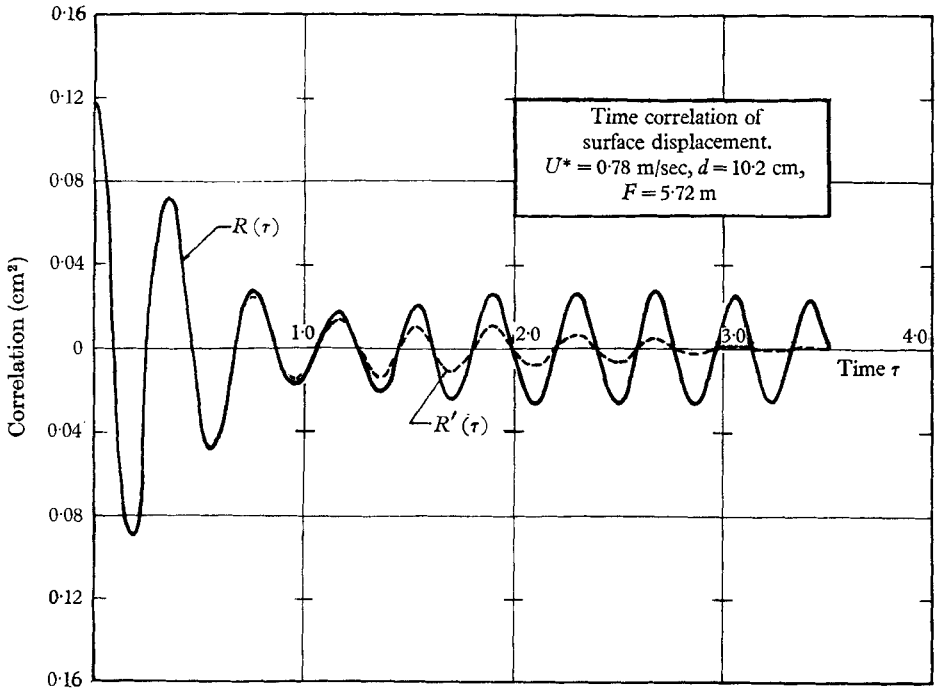

FIGURE 6. Typical unfaded and faded autocorrelation functions for the displacement of the water surface.

A typical example of $R(\tau)$ is shown in figure 6. As indicated $R(\tau)$ was generally found to oscillate regularly about the $R(\tau) = 0$ line with increasing τ. Its amplitude decreased sharply initially, but it became fairly steady at higher values of τ, though sometimes it varied slowly as if a lower harmonic was present.

The energy spectra were calculated by means of the following relation

$$\Phi(f) = \int_0^\infty R(\tau) \cos 2\pi f t \, dt. \tag{2}$$

The scheme for evaluating the integral in (2) for a finite record is given by Blackman & Tukey (1958). However, instead of the usual technique of 'hanning', it was preferred to obtain a suitable lag window by multiplying the function $R(\tau)$ by

$$g(\tau) = 1 + \cos(\pi\tau/T_m), \tag{3}$$

where T_m for our data is 3·5 sec. The fading function $g(\tau)$ has the advantage of suppressing the periodic component in the autocorrelation function at large lags without removing any information at short lags. An example of the faded autocorrelation $R'(\tau) = g(\tau).R(\tau)$, corresponding to the curve of $R'(\tau)$, is shown in figure 6. The spectrum corresponding to the faded autocorrelation $R'(\tau)$ of figure 6 is given in figure 7. This spectrum shows definite secondary peaks which correspond to the frequencies f_m where the spectral estimate is maximum.

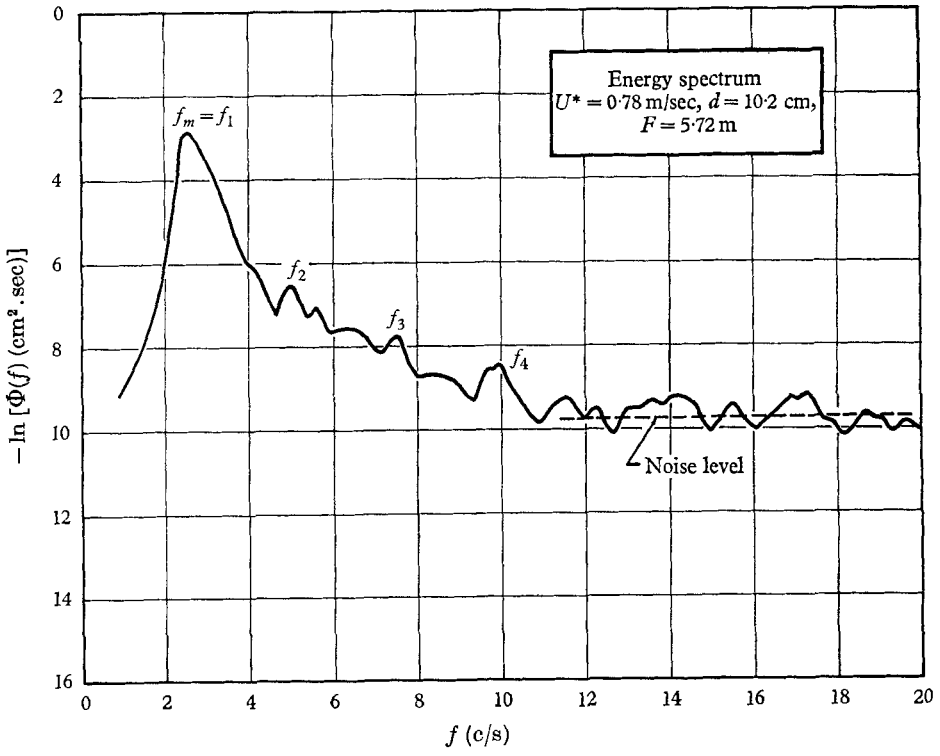

FIGURE 7. The energy spectrum corresponding to the faded autocorrelation in figure 5.

To be sure that the lag window given by (3) was not excessively distorting portions of the calculated spectra, the results using two other fading functions, $g = 1$, and $g = (1 - \pi\tau/T_m)$, were compared with the results of the cosine function in (3). The spectra calculated by the three different fading functions gave virtually the same spectral estimates for the particular cases examined.

The response of the water surface at a particular fetch to a step change in air flow indicated how the frequency spectra for the waves developed under duration-limited action of the wind. A typical set of amplitude spectra for growth

of waves with time on 10·7 cm deep water at a fetch of 4·8 m is shown in figure 8 (*a*). These data refer to the case where $U^* = 0{\cdot}52$ m/sec after the air flow reached conditions of steady flow. The spectral density function for surface displacement $\bar{\Phi}$, given in arbitrary units of (length)^2 sec, has been smoothed, and the noise level has been removed by the technique described by Hidy & Plate (1965*b*). The time written for the spectral curves in figure 8 (*a*) represents the arithmetic average of the time interval over the section of oscillograph record used to calculate the spectrum. The first interval of time started at the time the fan was started. During this experiment, the fan required about $2\frac{1}{2}$ sec to reach conditions of steady operating speed.

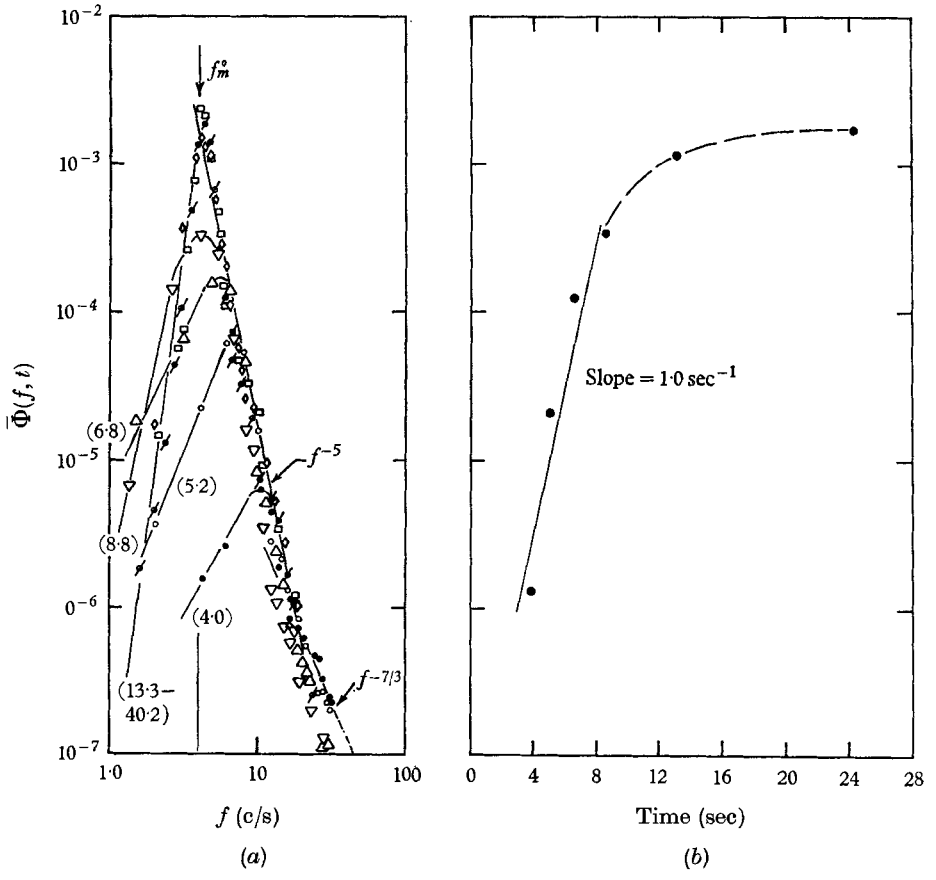

FIGURE 8. The transient growth of wind waves travelling down a channel. $U^* = 0{\cdot}52$ m/sec, and $d = 10{\cdot}7$ cm. (*a*) Calculated energy or amplitude spectra for wind waves observed at a given point in the channel. The fetch where these data were taken was 4·8 m. (*b*) The growth with time of a particular component of the spectra corresponding to the one whose $f_m = f_m^0$.

	time (sec)		time (sec)
●	4·0	⌀	13·3
○	5·2	◇	24·2
△	6·8	□	40·2
▽	8·8		

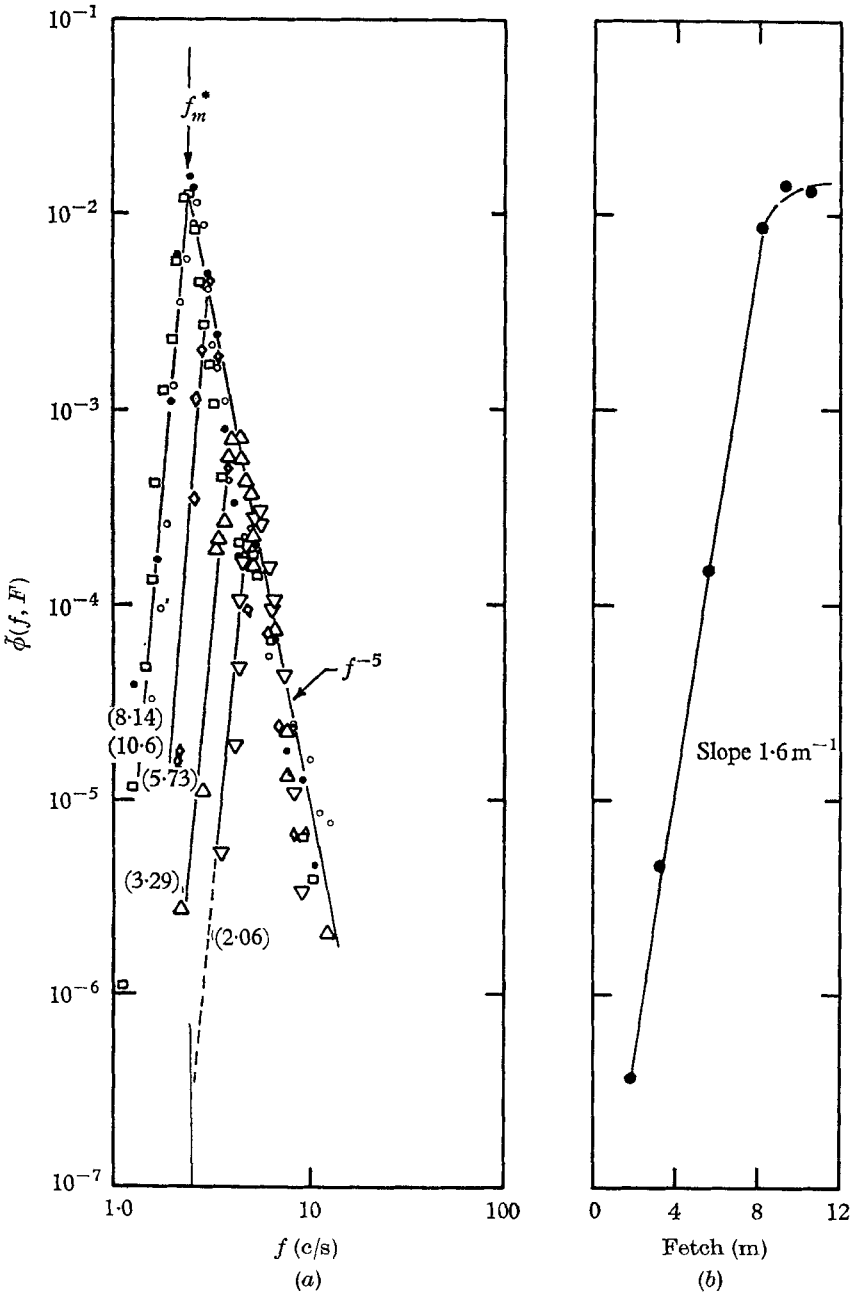

FIGURE 9. The development with fetch of wind waves under conditions of a steady wind blowing over a water surface. $U^* = 0{\cdot}50$ m/sec and $d = 10{\cdot}2$ cm. (*a*) Calculated energy or amplitude spectra for different values of fetch. (*b*) The development with fetch of a particular component of the spectra corresponding to the component whose $f_m = f_m^*$.

	Fetch (m)		Fetch (m)
▽	2·06	○	8·14
△	3·29	●	9·40
◇	5·73	□	10·6

In the early stage of development of the duration-limited wave pattern, the observed spectra contain little energy, and are rather broad. With increase in time after the start of the fan, the amount of potential energy in the waves increases, the spectra tend to become more peaked, and the frequency f_m where Φ is maximum shifts to lower values.

Typical frequency spectra for waves growing at increasing fetch under conditions of steady air flow, corresponding to the fetch-limited development, are shown in figure 9 (*a*). These data also were smoothed and corrected for noise level in the same manner as the duration-limited results. In figure 9, the notation $\tilde{\phi}$ is used to distinguish between the spectral density function for fetch-limited results and the duration-limited results, given by Φ.

At very short fetch, near the leading edge of the water, the observed spectra for fetch-limited development contain little energy, which is spread over a relatively wide range of frequency. As the waves travel downstream, the magnitude of the spectral density function increases, particularly in the low frequencies. The primary peaks of the spectra tend to sharpen up while the values of f_m decrease. These examples of spectra clearly show the similarity in development of waves under fetch-limited conditions and duration-limited conditions.

The potential energy taken at constant frequency in the spectra tends to reach an equilibrium level especially in the higher frequency levels. In the lower frequencies, components appear to have an exponential growth rate over a considerable range of time or fetch as illustrated for the duration-limited conditions in figure 8 (*b*), and for the fetch-limited case in figure 9 (*b*). Here the logarithm of the spectral density functions for the component of the spectrum corresponding to f_m at the longest interval of time shown as f_m^0, or the longest fetch attainable in the tunnel as f_m^*, is plotted respectively with time and with fetch. In the example shown in figure 8 (*b*), the increase of potential energy in the 4 c/s component was nearly exponential up to a time of approximately 8 sec. Similarly, the 2·4 c/s component in figure 9 (*b*) essentially grew exponentially up to a fetch of about 7 m.

4. Discussion

4.1. *Air flow and the stress on the water*

The interaction between the air and the water motion is reflected largely in the surface stress, τ_s. The average stress can be estimated from the set up, or slope of the water surface S, and the pressure gradient in the air dp/dx, using a momentum balance on the body of water standing in the tunnel. If the fluid motion is assumed to be two-dimensional, the average of the sum of the surface stress τ_s and the stress at the tunnel bottom τ_b is

$$\overline{(\tau_s+\tau_b)} = \rho_W g d[S+(\rho_W g)^{-1}(dp/dx)], \tag{4}$$

where ρ_W is the density of water, and g is the gravitational acceleration. In deriving this equation, the momentum change due to a change in water velocity, du/dx, is neglected. Ursell (1956) has pointed out that this omission might cause a significant error in estimating $\overline{\tau_s+\tau_b}$. However, when the necessary correction was calculated from experimental data obtained in the CSU tunnel by Goodwin

(1965), the modification for du/dx amounted to less than 1 % of the total shearing stress.

Equation (4) is not sufficient to calculate the surface stress. A second relation between $\bar{\tau}_s$ and $\bar{\tau}_b$ is needed, which was determined by Keulegan (1951) for laminar flow of water. He found a value of 1·50 for the ratio of $\bar{\tau}_s/\bar{\tau}_b$, and he estimated this ratio to be 1·25 for turbulent motion in the water. Francis (1951), however, found that $\bar{\tau}_s/\bar{\tau}_b$ is smaller than 1·25 for conditions of turbulent-water motion. More recent evidence of Baines & Knapp (1965), confirming Francis's conclusions, indicates that $\bar{\tau}_b$ is less than 10 % of $\bar{\tau}_s$ for cases of turbulent channel flow. Based on these results, $\bar{\tau}_s$ has been estimated for the purposes of this study from equation (4) by disregarding both the contribution of $\bar{\tau}_b$, and the effect of momentum changes.

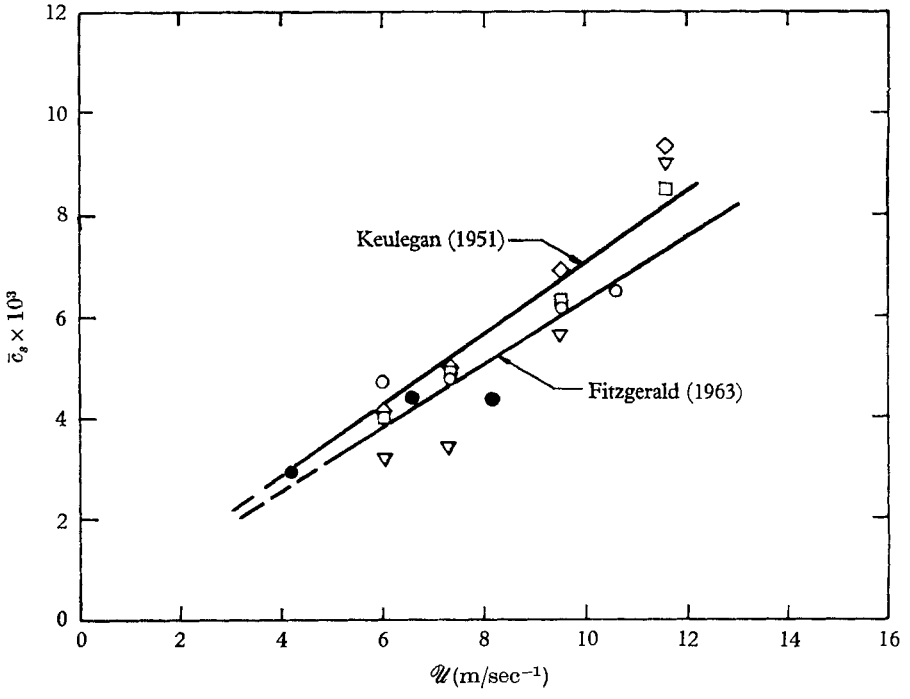

FIGURE 10. The variation of the mean stress coefficient with average wind speed.

		d (cm)
○	WB	5·1
□	WB	7·6
◇	WB	10·2
▽	WB	12·7
●	$\bar{c}_s$	10·2

The data for $\bar{\tau}_s$ are presented with corresponding values of Keulegan (1951) and Fitzgerald (1963) in figure 10. The surface stress is presented as an average friction coefficient defined by

$$\bar{c}_s = \bar{\tau}_s/\rho_A \mathscr{U}^2, \tag{5}$$

where ρ_A is the density of air.

To be consistent with Keulegan and Fitzgerald, our results have been referred to a cross-sectional average velocity $\mathscr{U}$ for the air. This reference velocity has been calibrated carefully with U_∞ in the CSU tunnel. For our data, $\mathscr{U}$ has been taken as $0{\cdot}80U_\infty$.

The results of our experiments, measured at several water depths, show scatter but generally they are quite close to the experimentally derived curves of both Keulegan and Fitzgerald. The systematic deviation of our data for the depth of 12·7 cm may not be significant because the slope of the water surface was very small in this case, and S could not be determined accurately at this depth.

As observed by other investigators, the average friction coefficient increases approximately linearly with wind speed over a fairly wide range of air speed. However, there may be a tendency for the friction coefficient to increase more rapidly than the linear value at the highest range of $\mathscr{U}$. In any case, the relation in figure 10 can be written as

$$\bar{\tau}_s = \rho_A \bar{c}_s \mathscr{U}^2 = 6{\cdot}67 \times 10^{-4} \rho_A \mathscr{U}^3, \tag{6}$$

which corresponds to an arithmetic average between the curves of Keulegan and Fitzgerald.

Since the technique of estimating the surface stress from equation (4) may be questioned, it is desirable to check independently the results shown in figure 10 using the measurements of the vertical profiles of air velocity. Local values of the friction coefficient c_s can be estimated from the growth of the boundary layer in the air by the momentum integral equation

$$c_s = \frac{\tau_s}{\rho_A U_\infty^2} = \frac{1}{U_\infty^2}\left[\frac{d}{dx}(U_\infty^2 \theta) - \frac{\delta^*}{\rho_A}\left(\frac{dp}{dx}\right)\right], \tag{7}$$

where θ is the momentum thickness and δ^* denotes the displacement thickness, defined in the usual way (e.g. Schlichting 1960).

To estimate the values of c_s from equation (7), the slope of $U^2\theta$ and the values of δ^* must be well estimated. The region of the vertical profile of velocity where the curvature is greatest makes the largest contribution to the values of θ and δ^*. In this study the portion of $U(z)$ that changed sharply lay too close to the water surface for accurate measurement with the fixed probe. Hence no completely reliable velocity estimates are available for this region, and the use of equation (7) consequently may be expected to give only a first approximation of the local friction coefficients.

In addition to the problem of using the experimental data in equation (7), the proper definition of a reference velocity presents difficulties. Equation (7) applies to flow over a solid boundary. When the boundary has translational flow and waves are superimposed on this motion, the air speed relative to fixed co-ordinates may be incorrect for defining the vertical profile to be used in equation (7). At least two other systems of velocity co-ordinates may be chosen. The air velocity relative to the surface drift may be a better system, or, as Benjamin (1959) has noted, the motion relative to the phase speed of waves may be more useful than the fixed system of reference. Introduction of either one of these reference systems will affect the definitions of θ and δ^*.

In spite of these difficulties, it is useful to apply (7) to obtain an independent estimate of average values of the friction coefficient. Hence, calculations of c_s were made based on the data for $U(z)$. Using $\mathscr{U} = 0{\cdot}8U_\infty$, an average coefficient then was estimated from the calculations from equation (7). Seven values at 1·5 m intervals along smoothed curves of c_s and U_∞ were chosen, and were averaged for three different cases. The resulting values of $\bar{c}_s$ are shown with the data in figure 10. The average coefficient of friction evaluated by the methods of equations (4) and (7) checks satisfactorily.

These results provide further evidence that the shearing stress along a smooth bottom for turbulent flow of water in a channel is a small part of the total average shearing stress as evaluated over the range of $4 < U_\infty < 16$ m/sec.

Local coefficients of friction and the logarithmic profile. The technique based on equation (4) gives satisfactory results for the average stress acting on the water. However, this method is not very suitable for determining local coefficients of friction because of the difficulties in measuring small changes in set up and pressure gradient over small distances in the channel. Nevertheless, our results for the mean stress, taken in a channel of 14 m length, are essentially the same as those of Keulegan using a narrower channel of 30 m length, and those of Fitzgerald, who used a channel of 4·5 m length. Therefore, it should be possible as an approximation to use an equation like (6) for different fetches, provided a suitable reference velocity for the air is chosen. In wind tunnels where the flow is not fully developed, the average velocity taken over a given cross-section has less meaning than the velocity associated with the region of potential flow U_∞, taken outside the developing layers along the walls, the bottom and the top of the tunnel. If we assume that (6), converted to refer to U_∞ rather than $\mathscr{U}$, represents the local values of the surface stress, the friction velocity in m sec^{-1} can be written as

$$U^* = (\bar{\tau}_s/\rho_A)^{\frac{1}{2}} = (3{\cdot}41 \times 10^{-4} U_\infty)^{\frac{1}{2}} U_\infty. \tag{8}$$

The air flow over the wavy water surface in the tunnel should correspond approximately to turbulent flow over a rough boundary. That is, the vertical distribution of air velocity near the water should be related to a form of the well-known 'law of the wall', such as

$$U = U^* \kappa^{-1} [\ln (z/z_0)], \tag{9}$$

where z_0 denotes the roughness length, and κ is Karman's constant, assumed equal to 0·40. When values of U^* are estimated from (8), the velocity profiles can be presented in the form of (9), and the magnitudes of z_0 can be calculated. The resulting dimensionless profiles of velocity for three classes of U_∞ are plotted in figure 11. The appropriate parameters for these results are tabulated in table 1 with corresponding values of the fetch, σ, the ratio (gz_0/U^*) and the roughness Reynolds number, $(U^* z_0/\nu_A)$. Although the logarithmic profile does not fit our data over the entire range of z, it correlates the results satisfactorily in the air layer near the water surface.

The roughness Reynolds number is rather small in the lower velocity range for classifying this first group of results as flow over a fully roughened surface.

Nevertheless, these data seem to fit the form of (9) just as well as the data for higher air speeds.

The motion over a fully rough surface should not depend on viscosity. As a consequence, Charnock (1955) has suggested on dimensional grounds that the ratio $(z_0 g/U^{*2})$ should be constant for fully rough flow. The values of this ratio,

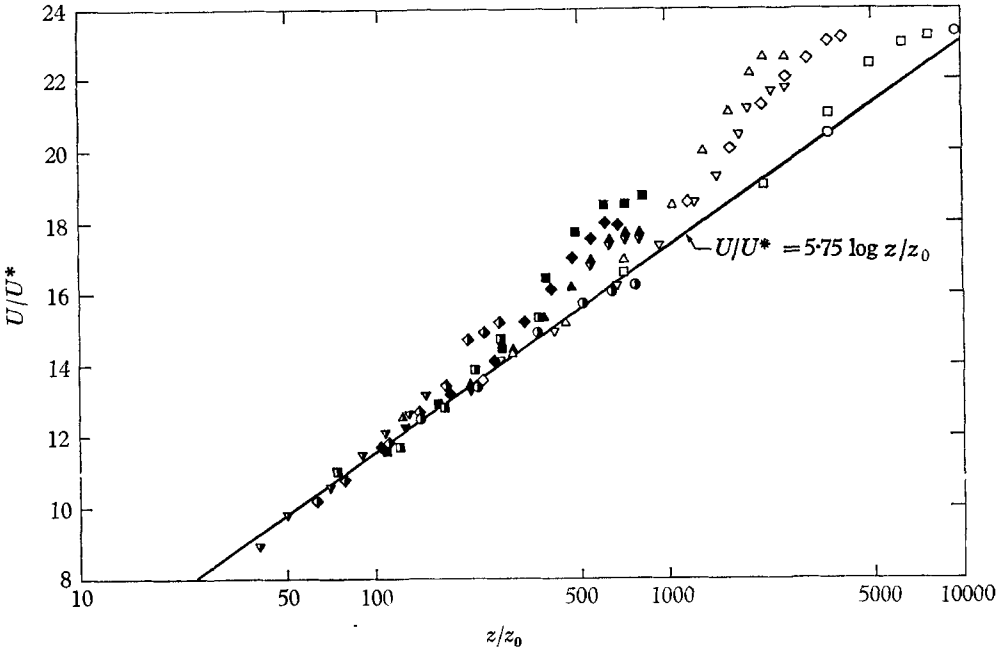

FIGURE 11. Dimensionless velocity distribution for air flowing over waves in a tunnel.

	U_∞ (m/sec)		
F(m)	6·1	9·4	14·8
2·1	○		◑
4·5	□	■	◨
6·9	◇	◆	◆
9·4	△	▲	
11·8	▽	▼	▽

as shown in table 1, tend towards a constant equal to 0·011 after a fetch of ~ 4 m. However, the approach of $(z_0 g/U^*)$ to a constant value does not seem to have any direct connexion with the roughness Reynolds number.

The fact that the roughness length increases with both U^* and σ implies that z_0 may be related to a Reynolds parameter based on U^* and σ. As indicated in figure 12, the logarithm of z_0 correlates quite well with the logarithm of $(U^*\sigma/\nu_A)$. This result is consistent with that of Kunishi (1963), who suggested that the aerodynamic roughness of wavy surfaces is related to a characteristic wave height when the waves are small, and they move at speeds much less than the mean air speed.

	F (m)	U_∞ (m/sec)	U^* (m/sec)	$z_0 \times 10^3$ (cm)	σ (cm)	$(gz_0/U^{*2}) \times 10^3$	$(U^* z_0/\nu_A)$	$(U^*\sigma/\nu_A)$
1	2·10	4·78	0·195	0·36	0·03	0·93	0·0382	3·22
	2·50	5·18	0·219	1·8	0·095	3·7	0·216	11·5
	4·90	5·46	0·238	5·4	0·20	9·3	0·705	26·2
	9·35	5·46	0·238	8·6	0·30	15	1·18	39·3
	11·8	6·09	0·278	9·4	0·39	12	1·41	59·6
2	2·50	7·83	0·415	23	0·31	13	5·23	70·6
	4·90	8·90	0·482	35	0·50	15	9·13	132
	9·35	9·25	0·523	30	0·62	11	8·3	178
	11·8	9·45	0·537	30	0·69	10	9·13	204
3	2·10	10·8	0·656	18	0·29	4·0	6·31	105
	2·50	12·1	0·785	52	0·64	8·3	22·4	276
	4·90	12·8	0·852	80	0·82	11	37·3	383
	11·8	14·8	1·06	127	1·03	11	74	600

TABLE 1. Parameters associated with the measurements of the vertical distribution of air velocity

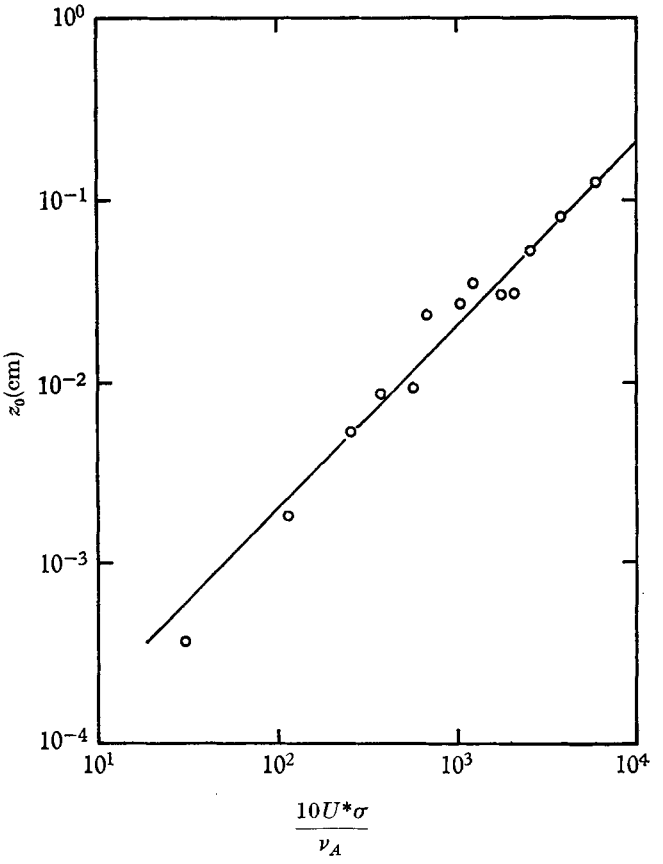

FIGURE 12. The variation in the aerodynamic roughness length with Reynolds number based on the friction velocity and the standard deviation of displacement of the water surface.

4.2. *The motion of the water*

When the experimentally determined values of $\bar{\lambda}$, σ, and $\bar{c}$ are compared with data obtained for small wind waves observed in other laboratory equipment (Wiegel 1961), and under natural conditions (Hicks 1963), close agreement between results is found. Detailed comparisons have been presented elsewhere by the authors (Hidy & Plate 1965*a*), hence further comparative discussion will not be considered here.

The wave speed and the drift current. The experimental values of the phase speed of significant waves were compared with estimates of the phase speed from the theory of infinitesimal waves. In all cases, the phase speed observed at a fixed point was greater than the corresponding theoretical value. It is clear, however, that such a comparison should be made after taking the relative motion of the water into account. If the water velocity is uniform, the phase speed $\bar{c}$ would be equal to the sum of the theoretical speed and the drift of the water. However, if the water velocity varies with depth, the theortical phase speed of waves must be corrected by some weighted average drift speed in the water, before comparison can be made with observations of $\bar{c}$, taken at a fixed location.

If the velocity distribution in the water is parabolic, Lilly (see appendix) finds that the phase speed measured at a fixed point should be related to the drift of the water surface u_0 and the theoretical phase speed of waves c_0 by the approximate equation

$$\bar{c} = c_0\left\{1 + \frac{u_0}{c_0}\left[1 + \frac{3}{2(\bar{k}d)^2} - \frac{1+2\cosh(2\bar{k}d)}{\bar{k}d\sinh(2\bar{k}d)}\right]\right\}, \tag{10}$$

where $\bar{k} = 2\pi/\bar{\lambda}$, and

$$c_0 = [(g/\bar{k})\tanh(\bar{k}d)]^{\frac{1}{2}}. \tag{11}$$

Using the values of u_0 from the measurements of particle trajectories, values of $\bar{c}$ were calculated for several cases by means of (10) and (11). Comparison between these values and corresponding experimental data showed an agreement between theory and observation with a fractional error of $\pm 15\,\%$. The range of error is approximately that expected on the basis of errors in estimation of $\bar{c}$ experimentally, and calculations of $\bar{c}$ theoretically using $\bar{\lambda}$ and u_0 in (10) and (11).

Systematic deviations between experimental values of $\bar{c}$ and those calculated from Lilly's relation might be expected, since both the effect of surface tension, and the effect of finite wave amplitude are not considered in deriving (10). The correction for surface tension in deep-water waves was found to be negligible for the experimental observations. However, the Stokes correction of $\bar{c}$ for gravity waves having finite amplitude as given by Lamb (1932) could result in values of the phase speed that are 1 to 11 % larger than c_0 if the amplitude of significant waves is 3σ. Thus Lilly's equation would give values of $\bar{c}$ somewhat larger on the average than the experimental data if the finite-amplitude value were substituted for c_0.

The effect of finite amplitude in the waves may be offset partially by the influence of turbulence in the water. Dye traces of the motion in the water indicated that the water flow was turbulent and not laminar. Therefore, the parabolic profile assumed in (10) does not strictly apply to our results. The use of a turbulent velocity profile having a steeper gradient near the surface than the parabolic curve, but having the same drift velocity at the surface, would result in a smaller correction factor for drift than that predicted by (10).

The drift on the water surface and the wind. Experimental results for the ratio $\gamma = u_0/\mathscr{U}$ have been obtained by Keulegan (1951) and Masch (1963) using the technique of tracing buoyant particles. Their observations indicated that γ is about 0·02, with a slight increase with Reynolds number based on the water depth and the drift velocity u_0. The ratio γ as determined from our data has an average value of about 0·017. The difference between these results probably can be accounted for as partly due to the effect of differences in air density between laboratories, and partly due to the effect of different (finite) sizes of the tracer particles being used by the different investigators. Since the buoyant particles are partially submerged in the water, their velocity is an average over the depth of submergence. The velocity gradient in the water is probably very steep, so that the average speed of particles of different size can change considerably the observed value of γ.

The tracer technique using the buoyant particles involves unresolved questions

about the statistical relations between the Lagrangian trajectories and the Eulerian velocity field. Therefore, though the statistical error in γ probably is small, the values of the drift velocity reported by us, and by Keulegan and Masch, are likely to be only first approximations to the actual values of u_0 and γ. It is worth noting, however, that an Eulerian theory of Lock (1951) predicts $\gamma \approx 0{\cdot}025$ for a steady interacting laminar flow between air and water. Although the analysis has limited applicability to our conditions of flow, it suggests that the magnitude of γ based on the tracer study may be quite reasonable.

Features of the autocorrelation functions. The autocorrelation functions for surface displacement displayed regular oscillations about $R(\tau) = 0$. The autocorrelation of a periodic function of period P is represented by another periodic function with the same period and zero mean. Therefore, the observed autocorrelation functions for the wavy surface evidently contain a quasi-periodic component which is related to the properties of the significant waves. Superimposed on the 'significant' periodic waves are random components which are

Case	$\bar{c}/\bar{\lambda}$	P^{-1}	f_m
21	2·74	2·87	2·91
79	4·62	4·83	4·74
100	5·61	5·71	5·65
113	2·91	2·85	2·76
169	3·24	3·31	3·26

TABLE 2. Comparison between frequency of significant waves in cyc/sec as estimated from the ratio $\bar{c}/\bar{\lambda}$, from $R(\tau)$, and from $\tilde{\phi}(f)$.

responsible for large values of $R(\tau)$ near $\tau = 0$. The period of significant waves thus should correspond to the period P of the oscillations at large values of τ. Typical values of P^{-1} calculated at large τ from curves of $R(\tau)$ are listed in table 2. Assuming that the frequency f_m, where the maximum in the spectrum occurs, represents the frequency of significant waves, f_m $(= P^{-1})$ also can be compared with $\bar{c}/\bar{\lambda}$. Typical examples of f_m and $\bar{c}/\bar{\lambda}$ are shown with P^{-1} in table 2. These three estimates of the frequency f_m are approximately equal for corresponding cases. Thus, the waves in the tunnel may be characterized essentially in terms of the properties of the significant waves.

The shape of the spectrum of waves. Energy that is transferred from the air to the waves is partially balanced by the dissipation of energy in the water motion. The wind action tends to increase the amplitude of smaller waves most rapidly, but the dissipation is also most pronounced in the smaller waves. Consequently, an equilibrium between energy input and energy loss tends to develop first in the highest-frequency components. Since dissipation has a smaller influence the smaller the frequency of waves, the lower-frequency components continue to absorb energy to higher levels before reaching equilibrium. Qualitatively, this simple model for the balance between the energy transferred to individual wave components and dissipation seems to explain the observed appearance and development of the spectra of the small wind waves.

If the only forces responsible for maintaining the wind waves at equilibrium are gravity and viscous forces, the equilibrium range of the spectrum should be proportional to f^{-5}, as shown on dimensional grounds by Phillips (1958*a*). At high frequencies of about 13 c/s, the effect of capillarity must become a primary influence on the wave behaviour. If an equilibrium spectrum exists in the range of $f > 13$ c/s, it may be governed by surface tension and viscosity only. Hicks (as quoted by Phillips 1958*b*) has suggested that under these conditions the equilibrium spectrum for capillary ripples should decrease with $f^{-7/3}$. Although capillary ripples appear to be generated continuously near the crest of bigger waves, one might expect that they would be damped out too rapidly by viscosity to approach equilibrium. There is some evidence, however, that the capillary wavelets at least attempt to approach an equilibrium distribution, as discussed earlier by the authors (Hidy & Plate 1965*b*).

The f^{-5} rule fits adequately the high-frequency range for the transient spectra even up to about 15–20 c/s (figure 8 (*a*)). Above this frequency range, the $f^{-7/3}$ rule seems to fit these data better than an f^{-5} decrease. The break from gravity-wave behaviour to capillary-wave behaviour should come at about 13 c/s for disturbances in deep water. Qualitatively, this frequency may be interpreted as the location of transition between the f^{-5} rule and the $f^{-7/3}$ rule in the spectra shown in figure 8 (*a*).

The frequency spectra for the fetch-limited cases have shapes similar to the transient data, and, as indicated in figure 9 (*a*), the equilibrium behaviour corresponding to the f^{-5} rule again appears in the higher frequencies up to about 15 c/s. Unfortunately, these data were taken in such a way that the noise level was too high for the potential energy in frequencies of about 15 c/s to be evaluated accurately. Therefore, the equilibrium range of capillary ripples could not be detected in this particular set of results.

In the frequency ranges below f_m, the data in figures 8 (*a*) and 9 (*a*) illustrate that there is a very steep forward slope in the spectral density functions up to the peak of the curves. This slope tends to increase with time up to a proportionality of $\sim f^8$, as indicated in figure 8 (*a*). After steady conditions of flow are reached, the forward slope tends to remain reasonably constant with fetch as shown in figure 9 (*a*). The steepness of the forward slope found in these results seems to be somewhat greater than found in spectra of wind waves generated on larger bodies of water. For example, Hicks (1963) found that the low range of the spectrum corresponds to $f^{1.3}$ for measurements taken on a lake at fetches less than 1000 m, while Burling's data (Hicks 1963) suggest a spectral density function proportional to $f^{6.6}$ for fetches of about 1000 m.

4.3. *The growth of waves in the tunnel*

The observed exponential growth of the lower-frequency components in the wave spectra is of some interest since these results qualitatively fit the predictions of recent shearing-flow theories for wave development. In particular, it seems useful to find out how well the theoretical calculations of Miles (1957, 1962*a*) and Benjamin (1959) fit the experimentally determined growth rates for waves in the tunnel.

Miles has discussed two alternative mechanisms for a shearing flow in air to induce wave growth on water. The first is an 'inviscid' mechanism which depends on the nature of the curvature of the mean vertical profile of air velocity in the region where the air speed equals the wave speed. The second mechanism, described also by Benjamin (1959), involves energy transfer to the water as a result of shear flow instability in the viscous layer next to the wavy surface. The wind waves generated in the tunnel are such that they move at a phase speed so small that the critical layer, in which $U = c$, lies in a region where the profiles of air velocity are nearly linear with height. This region, for example, lies at $z \approx 1$ cm in figure 3(*a*). For energy transfer from the air to the waves, Miles's (1957) inviscid mechanism requires some negative curvature in the velocity profile in the region where $U = c$. Therefore, this mechanism does not appear to play an important role in wave growth for the small waves observed in this study. However, the second mechanism dealing with the action of the air motion in the viscous layer seems to be applicable, and evidence for interpreting the growth of the wind waves in the tunnel by means of this theory is presented below.

In order for the mechanism of shearing flow instability to produce growth of waves, infinitesimal disturbances on the water initially must be present.

The initial perturbations of the surface may result from the action of pressure fluctuations in the turbulent air passing over the water, as proposed by Phillips (1957). Once the tiny ripples are generated by resonance interaction between the air pressure field and the water, the shearing flow mechanism can take over. Miles (1960) has combined Phillips's mechanism with his results to give a quantitative theory for the growth of waves over a limited range of time. Since this is a linear theory, it cannot account for non-linear effects which may contribute to the approach towards an equilibrium spectrum of waves. Therefore, Miles's combined mechanism cannot be expected to give a picture of wave development which is 'complete' for all times. In spite of this difficulty, it is worth while to investigate this theory's applicability to the range of experimental growth of wind waves on water in the laboratory channel.

After Miles (1960), the wave-number spectrum for the potential energy contained in gravity waves as measured at a fixed point has the form

$$\psi(\mathbf{k}, t) \sim \frac{\mathscr{F}}{2\rho_W^2 c_o^2(k)} \int_0^\infty \Pi(\mathbf{k}, T) \cos 2\pi f T \, dT. \tag{12}$$

For deep water waves, $f = (gk)^{\frac{1}{2}}$. The term $\Pi(\mathbf{k}, t)$ represents the spectrum for turbulent pressure fluctuations in the air. The parameter $\mathscr{F}$ reads

$$\mathscr{F} = (e^{2mt} - 1)/2m, \tag{13}$$

where t denotes the duration of wind action and m is the growth factor for waves of wave-number k (or frequency f).

Equation (13) indicates that, if $2mt \ll 1$, the growth of a particular component of the wavy surface is linear with time, as predicted by Phillips's (1957) theory. However, when $2mt \gg 1$, the growth of this component becomes exponential with time, which corresponds to the unstable growth discussed by Miles (1962*a*).

For the purposes of this discussion, we shall use the frequency spectrum Φ (or $\tilde{\phi}$) rather than the wave-number spectrum ψ. On dimensional grounds, for infinitesimal waves

$$\Phi(f,t) \sim (f^3/g^2)\,\psi(\mathbf{k},t), \tag{14}$$

or

$$\Phi(f,t) \sim \alpha(\mathbf{k},t)\,F(m,t), \tag{15}$$

where

$$\alpha = \frac{f^3}{(\rho_W g c_0)^2}\int_0^\infty \Pi(\mathbf{k},T)\cos 2\pi f T\,dT. \tag{16}$$

As an approximation, we assume that the integral of the pressure spectrum taken at a fixed point for the air flow in the tunnel in (16) is constant. Then the change of $\ln\Phi$ with time is

$$S_T = \partial \ln \Phi/\partial t = 2m\,e^{2mt}/(e^{2mt}-1). \tag{17}$$

For the cases $2mt \gg 1$

$$S_T \approx 2m, \tag{18}$$

and for $2mt \ll 1$

$$S_T \approx (1/t) + 2m. \tag{19}$$

Equations (17)–(19) should apply to the transient response of the water surface after air begins to flow down the tunnel. A relation similar to these equations should be applicable to the differences in the frequency spectra in the fetch-limited régime. Under these conditions, we shall assume that the integral of pressure fluctuations is independent of fetch and is constant. To use the analysis for changes in the spectrum with time for the case of variation with fetch, the dynamic transformation suggested by Phillips (1958*c*) is applied. Accordingly, the time of development to a given fetch for a wave of frequency f is

$$t = 2F/c_0(f). \tag{20}$$

With (20) the slope S_F of the curve for logarithm of $\tilde{\phi}$ vs. F for a particular frequency component is

$$S_F = \frac{\partial \ln \tilde{\phi}}{\partial F} = \left(\frac{4m}{c_0}\right)\left(\frac{\exp(4mF/c_0)}{\exp(4mF/c_0)-1}\right). \tag{21}$$

Hence, for $4mF/c_0 \gg 1$, the slope of the $\ln\tilde{\phi}$ vs. F curve should be approximately constant:

$$S_F(f) \approx 4m/c_0(f). \tag{22}$$

On the other hand, when $4mF/c_0 \ll 1$, the slope should vary with fetch as

$$S_F \approx F^{-1} + (4m/c_0). \tag{23}$$

Checking the Miles–Phillips theory. If the waves in the channel grow initially by interaction of the surface with the pressure fluctuations in the air, and later by shearing flow instability, certain qualitative observations should fit the experimental observations. For example, Phillips's (1957) mechanism for energy transfer to the water through oscillations in the air pressure suggests that the initial wavelets should have a frequency primarily around 13 c/s. Although all the components of waves on the water should be excited, the ripples in the range of 13 c/s should be most prevalent initially as a result of resonance

between the pressure fluctuations in the air and the water surface. This prediction can be tested by examining the frequency of wavelets appearing at very short times, or at a very short fetch. An extrapolation of the frequency, where the spectrum is maximum back towards zero time or zero fetch, should indicate the range of frequencies in which most of the energy was initially concentrated. Extrapolation of typical values of f_m from different spectra is shown in figures 13 and 14. These curves suggest that the energy contained in the initial disturbances on the water was maximum around frequencies of 12–15 c/s, as expected if Phillips's mechanism was responsible for the beginnings of wave growth.

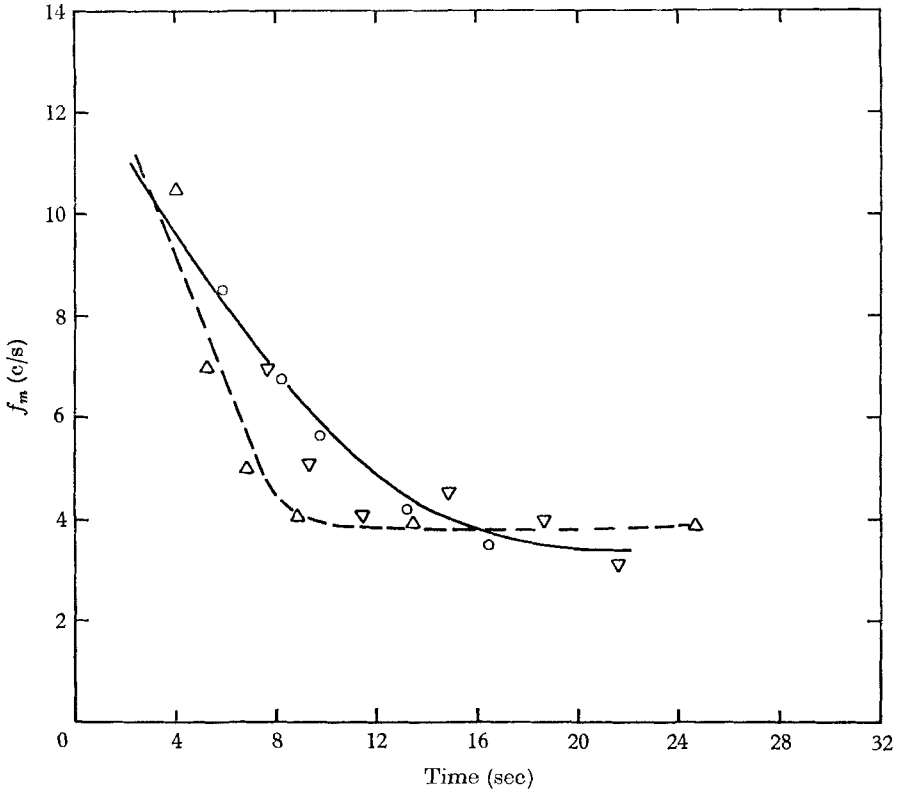

FIGURE 13. The change with time in the frequency where the energy spectrum of the waves has a maximum.

	U^* (m/sec)	d (cm)
○	0·54	10·7
△	0·68	10·7
▽	0·32	10·7

Phillips's theory considers the development of waves on water taken as infinite in all directions. Hence, waves can be generated by this mechanism which travel at all angles to the direction of the mean wind. However, the theory indicates that waves grow most rapidly at small angles to the wind direction. In the tunnel, the wind waves are restricted in their direction of propagation by the

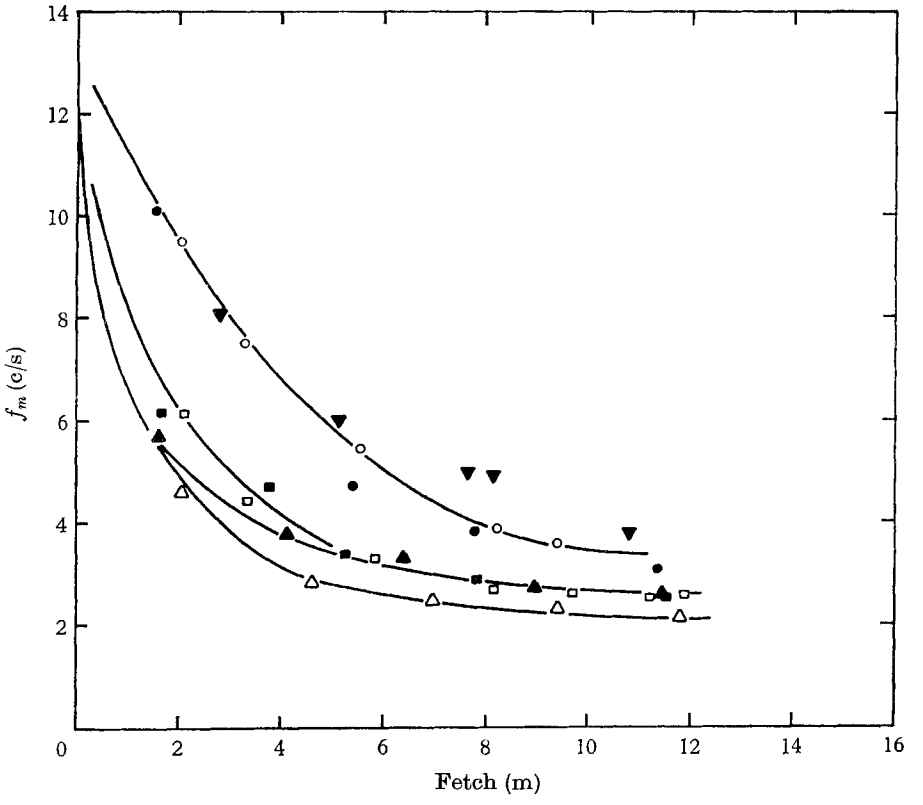

FIGURE 14. The change with fetch in the frequency where the energy spectrum of the waves is maximum.

	U^* (m/sec)	d (cm)
○	0·27	10·2
●	0·27	2·5
△	0·79	10·2
▲	0·79	2·5
□	0·54	10·2
■	0·54	2·5
▼	0·18	2·5

walls to move down-wind. The large waves in the channel tended to exhibit a two-dimensional character, and their crests travelled essentially normal to the wind direction. However, very near the leading edge of the water at low wind speeds, and at short running times, a three-dimensional mottled character was present on the water surface. Under these circumstances, small ripples were observed to travel short distances in all directions, but they moved primarily in the direction of the mean air flow. Thus, these observations again are qualitatively consistent with the Miles–Phillips picture.

The Miles–Phillips theory also predicts that there should be a transition between a linear growth of ripples and an exponential growth of waves, as indicated in (17)–(19) and (21)–(23). A criterion for the zone of transition

based on the 'inviscid' Reynolds stress theory of Miles (1957) has been established by Phillips & Katz (1961). The region of transition is associated with certain values of the ratio $F/\overline{\lambda}$, and the ratio $\bar{c}/U_\infty$. The curve for transition as predicted by Phillips & Katz for waves propagating in the direction of the mean wind is shown in figure 15. The blocks of data of three different workers, as discussed by Phillips & Katz, are also indicated with the theoretical curve. Some points calculated from our results are plotted in this figure. These data are qualitatively in agreement with the predictions of the Miles–Phillips mechanism, and they are consistent with other investigators.

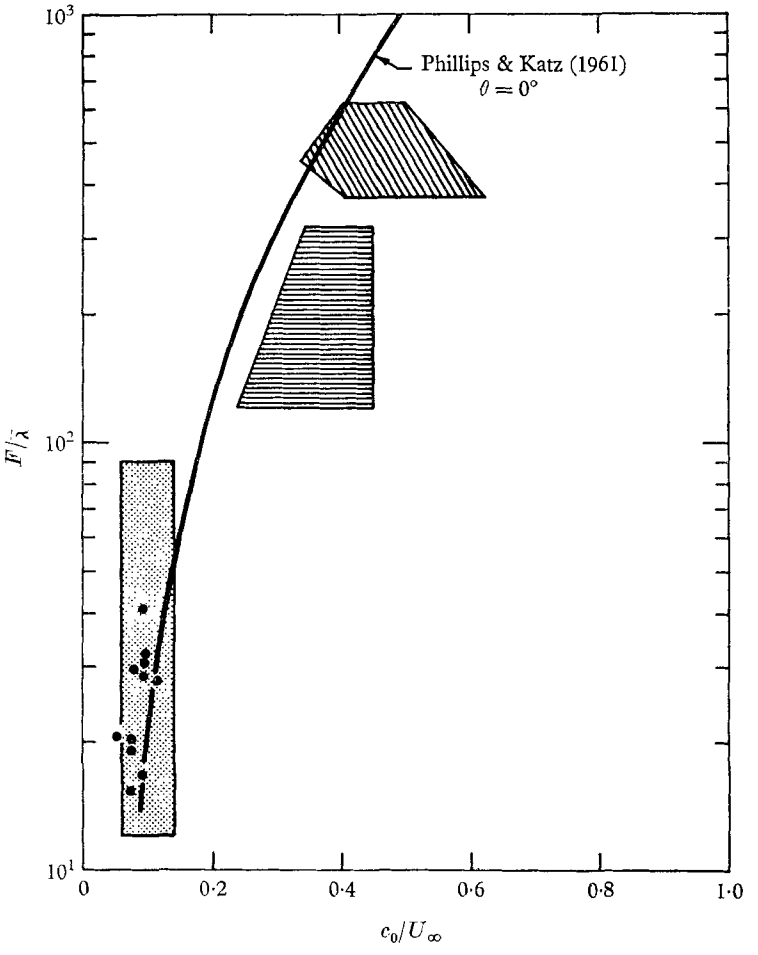

FIGURE 15. Conditions of transition between models for growth of wind waves (after Phillips & Katz 1961). ●, This study; ⊟, Burling; ▨, Kinsman; ▦, Pierson.

The frequency component in the spectra that will exhibit exponential growth over the widest range of time or fetch corresponds to the component whose potential energy is greatest at long times, or at maximum fetch in the tunnel. These components have been chosen for the curves in figures 8(*b*) and 9(*b*). In both of these cases a rather wide range of exponential growth is found before

equilibrium is reached. If the Miles–Phillips theory is applicable to these results, the slopes should be predictable from this theory using the estimates of the growth factor m from Miles's (1962*a*) calculations.

The net growth factor is given by

$$m = m_A + m_W. \tag{24}$$

The damping coefficient reads

$$m_W = 2k^2\nu_W - (2k^3\nu_W c_0)^{\frac{1}{2}}\, e^{-2kd}, \tag{25}$$

where ν_W is the kinematic viscosity of water. If the non-dimensional parameter

$$z' = k^{\frac{1}{3}} c_0\, \nu_A^{\frac{1}{3}}/U^{*\frac{4}{3}} \tag{26}$$

is much less than unity, then Miles's (1962*a*) results show that

$$m_A \approx \left(\frac{\rho_A}{\rho_W}\right) kU^* \left[\frac{0{\cdot}322}{w^2}\left(\frac{U^*}{k\nu_A}\right)^{\frac{2}{3}}\left(\frac{c_0}{U^*}\right) + \frac{0{\cdot}343}{w}\left(\frac{U^*}{k\nu_A}\right)^{\frac{1}{3}}\right], \tag{27}$$

where ν_A denotes the kinematic viscosity of air.

The parameter w is given by Miles (1962*b*) as

$$w = (\kappa c_0/U^*)\, W[R, \kappa(U_1 - c_0)/U^*], \tag{28}$$

and

$$R = \kappa(U^*/k\nu_A). \tag{29}$$

The dimensionless function W for the linear-logarithmic profile of air velocity has been tabulated by Miles (1962*b*).

According to Miles' calculations, the velocity U_1 refers to the speed at the edge of the viscous sublayer. Since the air flow over the water generally corresponded to fully rough conditions, the concept of a viscous sublayer in these experiments has a poorly defined meaning. It seems plausible, however, to assume that U_1 roughly can be related to the air speed at a height z equal to σ above the mean surface. Thus, one can estimate U_1 from (9) using the data for z_0 shown in figure 12.

Using the above expressions, the tables of Miles (1962*b*), and

$$\rho_A/\rho_W = 9{\cdot}95 \times 10^{-4}$$

at 293 °K, calculations of m were made for several cases of transient growth and growth with fetch for wind waves in the channel including those shown in figures 8(*b*) and 9(*b*). The values of U^* for each condition of U_∞ were estimated from (8).

The data for the growth factor m for three different transient cases are shown in table 3 along with corresponding values of U^*, z', and the parameters of the waves. The time t_0 (= 6·0 sec) was chosen arbitrarily to evaluate the slope of the curves of $\ln \Phi(f_m^0)$ vs. t. The values of the product $2mt_0$ tabulated in table 3 are all larger than unity so that the asymptotic expression (18) is applicable for estimating the slope of the curves shown, for example, in figure 8(*b*). Comparison between the expected slope of the estimated linear region, S_T, and the observed value S_E indicates an agreement within a factor of about three or

U^* (m/sec)	F (m)	d (cm)	f_m^0 (cyc/sec)	c_0 (m/sec)	$(\rho_A/\rho_W)U^{*2}/\nu_A k$ (m/sec)	z'	m (sec^{-1})	$2mt_0$	S_T (sec^{-1})	S_E (sec^{-1})
0·52	4·8	10·7	4·0	0·40	0·23	0·102	0·47	5·64	0·94	1·0
0·54	6·0	10·7	3·5	0·44	0·315	0·097	0·34	4·07	0·68	1·4
0·32	8·5	10·7	3·0	0·50	0·14	0·21	0·10	1·2	0·20	0·60

TABLE 3. Comparison between growth of wind waves with time and theoretical predictions

U^* (m/sec)	d (cm)	f_m^* (cyc/sec)	c_0 (m/sec)	$(\rho_A/\rho_W)U^{*2}/\nu_A k$ (m/sec)	z'	m (sec^{-1})	$4mF_0/c_0$	S_F (m^{-1})	S_E (m^{-1})
0·50	10·2	2·4	0·58	0·47	0·12	0·075	3·12	0·52	1·6
0·28	10·2	3·6	0·44	0·08	0·23	0·17	9·0	1·5	2·1
0·63	10·2	2·1	0·63	0·86	0·078	0·097	3·7	0·62	0·96
0·39	10·2	2·5	0·57	0·28	0·16	0·057	2·4	0·40	1·1
0·50	7·6	2·4	0·58	0·47	0·12	0·075	3·12	0·52	1·3

TABLE 4. Comparison between experimental growth of waves with fetch and theoretical predictions

less in all three cases. However, the theoretical slopes are systematically lower than the experimentally observed values.

There are a number of difficulties in using the spectra calculated from the transient records for testing the Miles–Phillips theory. In the first place, the waves grow in time very rapidly in the channel. At moderate wind speeds waves reach their steady-state amplitudes in a matter of a few seconds. Under these conditions the aliasing problems as discussed by Blackman & Tukey (1958) can become quite appreciable. Aliasing error can be reduced by using the Blackman & Tukey criteria for minimizing error. Furthermore, the values of f_m^0 are so small that the sections of record used for estimates of $\bar{\Phi}$ would allow passage of only 1 or 2 waves of frequency f_m^0 in the time of recording. This hardly corresponds to a satisfactory statistical sample for estimating the value of the spectral estimate in the lower range of frequencies. In addition, the values of U^* and σ depend on the water surface. Instead of remaining constant, U^* and σ will vary with time as the water waves grow. For these reasons, the transient data described here can provide only qualitative test of the Miles–Phillips mechanism, and only order-of-magnitude agreement between S_T and S_E can be expected.

The data taken for the fetch-limited cases are relatively free from the difficulties associated with the duration-limited results. The water surface displacement could be recorded for a long enough time to allow a good statistical sample to be taken. The values of U^* as estimated from (8) are directly applicable to this case, and there are no difficulties associated with the starting of the fan. Therefore, it is expected that the fetch-limited data should agree better with theoretical predictions, provided that the simple dynamical transformation of (20) is justified.

Calculations were made for several fetch-limited cases using (25) and (27), and the resulting data are tabulated in table 4. The slopes of the experimental curves such as the one in figure 9(*b*) were calculated arbitrarily at a fetch F_0 equal to 6 m. The ratios $4mF_0/c_0$ for the data in table 4 are appreciably larger than unity so that the assumed form of (25) is justified for estimating the slope S_F. Except for one example, the agreement between the theoretical values of the slope $S_F\,(=4m/c_0)$ and the experimental estimates S_E is satisfactory, considering the number of assumptions which have been made to obtain these results. However, it is observed that the theoretical estimates again are systematically less than the experimental results in the fetch limited cases as in the examples of the transient data shown in table 3.

Both the fetch-limited data, and the duration-limited data presented in this study exhibited only the exponential range of growth predicted by the Miles–Phillips model. The régime of linear growth and the transition range could not be detected in the results because the spectral estimates were too inaccurate at very small values of time interval and fetch, and too few data were available for conditions of initial development of the waves.

There are several points to be considered in explaining the differences between Miles's predictions based on (27), and the experimental results. First of all, Miles (1962*a*) notes that (27) only applies to conditions where $z' \ll 0{\cdot}1$, and to conditions where the ratio $[(\rho_A/\rho_W)\,U^{*2}\nu_A k]$ is less than $c_0(k)$. The conditions for

the first contingency are not met in the data presented in tables 3 and 4. The data presented in this study also do not follow the second restriction. Miles (1962*a*) notes that when $[(\rho_A/\rho_W)\, U^{*2}\nu_A\, k)] \approx c_0$, the Kelvin–Helmholtz mechanism (e.g. Lamb 1932) must be taken into account in the growth of waves. Miles (1959) suggests, however, that this mechanism may contribute only a small part to the overall energy transfer from flowing air to water waves. Nevertheless, the additional contribution of the Kelvin–Helmholtz mechanism to the process of energy transfer qualitatively helps to explain the higher values of S_E than predicted by Miles' theory alone.

In addition to energy transfer from the air to the water by the mechanisms discussed above, one should also consider the effect of a favourable pressure gradient in air acting on the waves. The observed systematic pressure decrease from the windward side to the leeward side of the waves (dp/dx) also should make a contribution to the process of energy exchange.

Consideration of the deviations between the theoretical estimates and the experimental results in tables 3 and 4 should also include a careful look at the damping term given by (27). Strictly speaking, the damping coefficient given in (27) should be modified for the flow in the channel. The additional viscous dissipation for waves propagating down a channel may result from the influence of the walls and the bottom of the channel. This additional dissipation has been estimated from a relation of Hunt (1952). The increased (laminar) dissipation for the rectangular channel as indicated by Hunt's equation was found to be negligible for the cases in tables 3 and 4.

Because the water motion was turbulent, another factor may have tended to increase dissipation. Phillips (1961) has given an estimate of the dissipation expected from turbulence induced by gravity waves. The application of his relation indicates that this mechanism produces only very small dissipation for the classes of waves studied in the channel.

It has been known for some time that traces of oil or other surface contaminants on a water surface can cause suppression of wave growth in excess of that produced by viscous damping alone. Although care was taken to minimize the contamination of the water in the CSU channel, and no slicks of oil on the surface were observed, very small amounts of oil unavoidably may have been present. The possible effect of surface contamination is difficult to estimate in these experiments. However, our observations of the onset under given wind conditions of the initial small ripples on water which had been standing in the channel for several days were identical with the results for fresh water. Therefore, the effect of surface contamination on the rate of dissipation of waves is believed to be negligible.

In explaining the sources for differences between theory and experiment, one also should consider that the flow of air and water in the tunnel had rather important three-dimensional characteristics. At a given fetch, the vertical distribution of air velocity varied across the tunnel. Although the waves tended to travel with straight crests oriented normal to the mean flow, some differences in the energy transfer from air to water across the mean flow were inevitable. This, of course, is not accounted for in Miles' two-dimensional theory.

Aside from the unknown effects of turbulence in the fluids, the only remaining mechanism that might explain the deviation between theory and experiment is the influence of non-linear interaction between different Fourier components of the wavy surface. Unfortunately, the magnitude of this effect is uncertain and at present is difficult to estimate for the results of this study.

One should bear in mind, of course, that the calculations based on Miles' (1962*a*) theory depend strongly on the arbitrariness of defining of the velocity U_1. The ambiguities in conceiving of a viscous sublayer near the water surface make a precise comparison between theory and experiment rather intractable.

5. Conclusions

Experimental measurements of a number of properties of the combined air and water motion in a laboratory channel have confirmed and extended the findings of other investigators. In particular, it was found that: (*a*) although the air motion in the channel followed a three-dimensional pattern characteristic of wind tunnels of rectangular cross-section, many features of the air–water flow could be described in terms of a two-dimensional picture; (*b*) the wind waves generated in the channel travelled downstream at approximately the same phase speed as gravity waves of small amplitude, provided the effect of the drift current was taken into account; (*c*) the average drag coefficients for the action of the wind on the water surface increased with increasing wind speed, and these data were essentially the same as the results of previous investigators; (*d*) the mean velocity profiles for the air could be placed in the framework of classical similarity theory, and the friction velocity and the aerodynamic roughness of the water surface were related to the height of the waves; (*e*) the autocorrelations of surface displacement and the frequency spectra were consistent with the visual observations that the wind waves in the tunnel consist of nearly periodic waves on which random wavelets are superimposed; (*f*) energy in the high-frequency range in the spectra approached an equilibrium distribution rather quickly, while the lower-frequency components initially grew exponentially with time and fetch, but later tended to approach a state of equilibrium.

The wave development in a laboratory channel can be explained reasonably well by a mechanism where the growth of waves is initiated by turbulent pressure fluctuations in the air flow over the water, and is augmented by energy transfer from the air to the water through shearing flow instability. The growth rate of a particular spectral component with time at a point, and with distance under steady flow conditions can be predicted generally within a factor of about two using recent theoretical analyses of Miles (1960 and 1962*a*). The deviations between the theoretical and experimental results can be explained primarily by the fact that the theory probably has only limited applicability to the experimental data.

The wind–water tunnel at Colorado State University was constructed under a matching grant from the National Science Foundation. This work was supported by the National Science Foundation in connexion with its grant to Colorado State University, and with its contract with the National Center for

Atmospheric Research. The authors appreciate the helpful comments of Profs O. M. Phillips and J. W. Miles. We are indebted to G. D. Hess for pointing out an inconsistency in the original manuscript.

Appendix: On the speed of surface gravity waves propagating on a moving fluid

BY D. K. LILLY

National Center for Atmospheric Research

The problem of surface waves moving on a moving fluid has been treated by several authors, including Abdullah (1949), Burns (1953), Hunt (1955) and Thompson (1949). Burns's work is most pertinent to the problem presented by the above results, but the solutions were restricted to shallow-water wave conditions. In the following, a method is presented suitable for obtaining wave speed solutions for any fluid velocity profile, so long as the maximum velocity difference within the fluid is much less than the wave speed. It is applied specifically to the case of a laminar parabolic flow profile with zero net transport, which may or may not be a good approximation to the conditions in the experiments reported above. If and when accurate water velocity profile measurements are made this method can be used to formulate a simple numerical integration scheme to find the desired result.

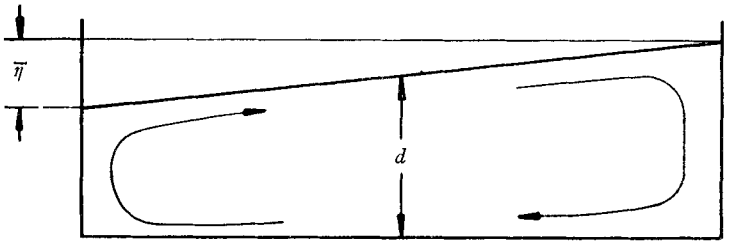

FIGURE 16. Schematic diagram of air–water interface in a channel. Wind blows from left to right, setting up surface displacement $\bar{\eta}$ and forward and return drift currents.

In the investigation reported in the above paper, Hidy & Plate found that the wave phase speed tended to be significantly greater than that predicted by linear theory. The effect of the downwind drift of the water surface would tend to add to the wave speed measured with respect to a fixed point, depending on the depth profiles of the drift current and wave amplitude.

We assume steady-state air flow over a sloping water surface exerting a constant stress τ_s on that surface. The water is bounded at both ends as in figure 16, so that the vertically integrated flow must vanish. If we avoid consideration of conditions near the lateral boundaries, the equation of motion may be written as

$$\nu_W \frac{d^2u}{dz^2} = \frac{1}{\rho_W}\frac{\partial p}{\partial x} = g\frac{d\bar{\eta}}{dx}, \tag{A 1}$$

where ρ_W, ν_W, p, and u are the water density, kinematic viscosity, mean pressure and drift current velocity, respectively, and $\overline{\eta}$ is the mean vertical displacement of the surface. The boundary conditions are

$$\rho_W \nu_W du/dz = \tau_s \quad \text{at} \quad z = \overline{\eta}, \tag{A 2}$$

$$u = 0 \quad \text{at} \quad z = -d. \tag{A 3}$$

The integral constraint is

$$\int_{-d}^{\overline{\eta}} u\,dz = 0. \tag{A 4}$$

Upon neglecting the value of $\overline{\eta}$ in (A 2) and (A 4) we obtain the usual parabolic form of laminar velocity distribution as follows

$$u = u_0(1 + 4(z/d) + 3(z/d)^2), \tag{A 5}$$

$$u_0 = \tau_s d/4\nu_W \rho_W, \tag{A 6}$$

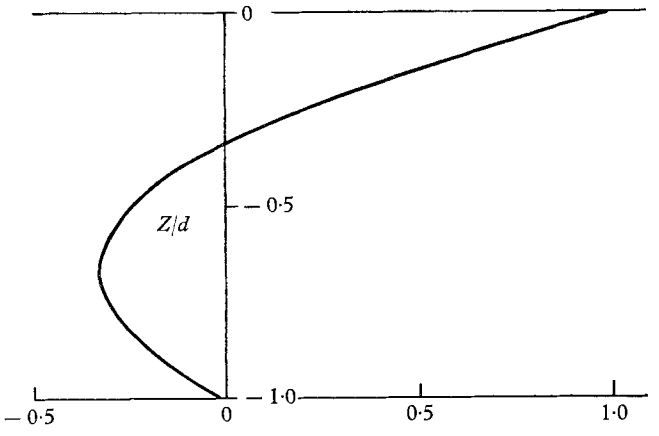

FIGURE 17. Profile of the dimensionless drift current u/u_0 as a function of dimensionless depth, z/d, from equation (A 5).

and the displacement height gradient is given by

$$S = d\overline{\eta}/dx = 3\tau_s/2\rho_W gd. \tag{A 7}$$

The profile, shown in figure 17, shows vanishing velocity at $z = -\frac{1}{3}d$ with a return flow below, having a maximum amplitude $\frac{1}{3}u_0$.

Upon forming the perturbation equations of the flow and performing standard reductions, we may obtain an equation for the vertical variation of the stream function as follows

$$(u-c)(\phi'' - k^2\phi) - u''\phi = 0, \tag{A 8}$$

with boundary conditions

$$\phi = 0 \quad \text{at} \quad z = -d, \quad (u-c)\phi' = (g/(u-c) + u')\phi \quad \text{at} \quad z = 0, \tag{A 9}$$

where

$$\psi = \phi(z)\, e^{ik(x-ct)} \tag{A 10}$$

is the stream function. It is difficult or impossible to find a solution to this set in closed form, with u replaced by (A 5); therefore we attempt a series approximation of the form

$$\phi = \phi_0 + \epsilon\phi_1 + \epsilon^2\phi_2 + \ldots, \tag{A 11}$$

$$c = c_0 + \epsilon c_1 + \epsilon^2 c_2 + \ldots, \tag{A 12}$$

where $\epsilon = u_0/c_0$ is assumed to be a small parameter. The normal gravity wave speed, c_0, will be obtained in the first approximation.

Upon substitution of (A 11) and (A 12) into (A 8) and equating terms of the same power of ϵ (u is of order ϵ) we obtain the following ordered system:

$$\left.\begin{aligned} &\phi_0'' - k^2\phi_0 = 0, \\ &\phi_1'' - k^2\phi_1 = -(u''/u_0)\,\phi_0, \\ &\phi_2'' - k^2\phi_2 = \ldots, \\ &\vdots \end{aligned}\right\} \tag{A 13}$$

in which all equations after the zeroth order have inhomogeneous terms of lower order. The boundary conditions similarly lead to the following relations:

$$\phi_0 = \phi_1 = \phi_2 = \ldots = 0 \quad \text{at} \quad z = -d, \tag{A 14}$$

$$\left.\begin{aligned} &\phi_0' - (g/c_0^2)\,\phi_0 = 0, \quad \text{at} \quad z = 0, \\ &\phi_1' - (g/c_0^2)\,\phi_1 = 2\left(\frac{u}{u_0} - \frac{c_1}{c_0}\right)\phi_0 - \frac{u'}{u_0}\,\phi_0, \\ &\phi_2' - (g/c_0^2)\,\phi_2 = \ldots. \end{aligned}\right\} \tag{A 15}$$

The zeroth-order solution of (A 13), (A 14) and (A 15) leads to the classical results for the stream function and wave velocity

$$\phi_0 = A\sin[k(z+d)], \quad c_0^2 = (g/k)\tanh(kd), \tag{A 16}$$

where A is an arbitrary constant. The first-order solution may be written in the integral form

$$\phi_1 = -k^{-1}\int_{-d}^{z} (u''/u_0)\,\phi_0 \sinh[k(z-z')]\,dz'. \tag{A 17}$$

Upon substitution of (A 16) and (A 17) into (A 9) and evaluation of the integrals, an expression for the first-order correction to the phase speed is obtained. For $u''/u_0 = 6/d^2$, from (A 5), the result may be expressed as

$$\frac{c_1}{c_0} = 1 - \frac{1 + 2\cosh(2kd)}{kd\sinh(2kd)} + \frac{3}{2k^2d^2}. \tag{A 18}$$

It is of interest to consider (A 18) for the limiting cases of deep-water ($kd \to \infty$) and shallow-water ($kd \to 0$) waves separately. For the shallow-water case we have

$$\frac{c_1}{c_0} \Rightarrow 1 - \frac{1 + 2(1 + 2k^2d^2 + \frac{2}{3}k^4d^4)}{kd\,(2kd + \frac{4}{3}k^3d^3 + \frac{4}{15}k^5d^5)} + \frac{3}{2k^2d^2} \Rightarrow \frac{k^2d^2}{5}. \tag{A 19}$$

That is, the correction tends to vanish. This is essentially because the energy density becomes constant with depth while the mean drift velocity vanishes. For deep water we obtain

$$c_1/c_0 \Rightarrow 1 - (2/kd). \tag{A 20}$$

In this case the phase-velocity correction approaches the surface current u_0, because the wave energy is entirely contained within the surface layer.

The solid curve in figure 18 is a plot of c_1/c_0 as a function of kd. The deep-water and shallow-water approximations are shown as dashed curves. For comparison the gravity wave velocity itself is plotted as the dash-dotted curve, with its deep- and shallow-water approximations also shown. Apparently there is a slight difference in interpretation of 'deep' and 'shallow' between the correction term and the unperturbed wave speed. Also it should be noted that there is a

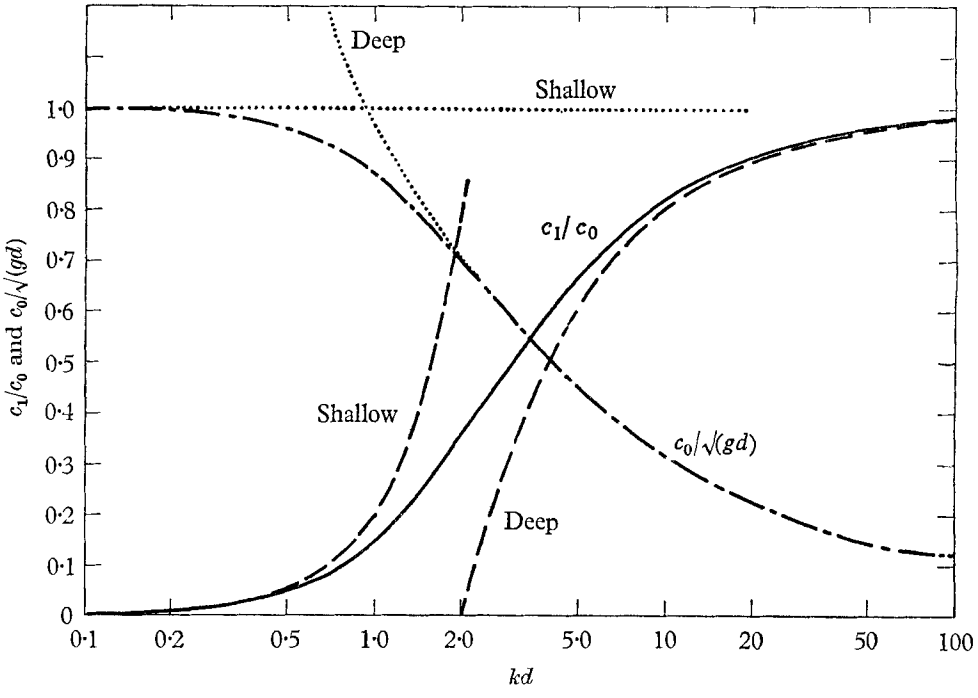

FIGURE 18. The solid curve, from equation (A 18), is the first-order drift current correction to the gravity wave velocity in non-dimensional units as a function of the product of wave number and depth. To obtain dimensional values, multiply by c_0. The dash-dotted curve, from equation (A 16), is the uncorrected gravity wave velocity as a fraction of $(gd)^{\frac{1}{2}}$. Deep- and shallow-water approximations are shown as dashed and dotted curves.

significant range of kd for which neither the deep- nor the shallow-water approximation is adequate. It is probable that the correction for an arbitrary velocity profile, say that prevailing in turbulent flow, would depend on wavelength and depth in a somewhat more complicated manner.

REFERENCES

ABDULLAH, A. J. 1949 *Ann. N.Y. Acad. Sci.* **51**, 425.

BAINES, W. D. & D. J. KNAPP 1965 *Proc. A.S.C.E. (J. Hydraulics Division)*, **91**, 205.

BENJAMIN, T. B. 1959 *J. Fluid Mech.* **6**, 161.

BLACKMAN, R. B. & TUKEY, J. W. 1958 *The Measurement of Power Spectra.* New York: Dover.

BURNS, J. C. 1953 *Camb. Phil. Soc.* **49**, 695.

CHARNOCK, H. 1955 *Q. J. Roy. Met. Soc.* **81**, 639.

FITZGERALD, L. M. 1963 *Aust. J. Phys.* **16**, 475.

FRANCIS, J. R. D. 1951 *Proc. R. Soc.* A, **206**, 387.

GOODWIN, C. R. 1965 The effect of wind drag on open-channel flow. Unpublished M.S. thesis, Colorado State University, Ft. Collins, Colorado.

HICKS, B. L. 1963 *Ocean Wave Spectra.* Englewood Cliffs. N.J.: Prentice-Hall.

HIDY, G. M. & PLATE, E. J. 1965*a* Laboratory studies of wind action on water standing in a channel. *ESSA (USWB) TN*, no. 9-SAIL-1, pp. 285–321.

HIDY, G. M. & PLATE, E. J. 1965*b* *Phys. Fluids* **8**, 1387.

HUNT, J. N. 1952 *Houille Blanche* **7**, 386.

HUNT, J. N. 1955 *Proc. R. Soc.* A, **231**, 496.

KEULEGAN, G. H. 1951 *Res. Nat. Bur. Stand.* **46**, 358.

KUNISHI, H. 1963 *Bull. Disaster Prev. Res. Inst.* no. 61, Disaster Prev. Res. Inst., Kyoto, Japan.

LAMB, H. 1932 *Hydrodynamics.* New York: Dover.

LOCK, R. C. 1951 *Q. J. Mech. Appl. Math.* **4**, 42.

MASCH, F. 1963 *Int. J. Water Air Poll.* **7**, 697.

MILES, J. W. 1957 *J. Fluid Mech.* **3**, 188.

MILES, J. W. 1959 *J. Fluid Mech.* **6**, 583.

MILES, J. W. 1960 *J. Fluid Mech.* **7**, 469.

MILES, J. W. 1962*a* *J. Fluid Mech.* **13**, 433.

MILES, J. W. 1962*b* *J. Fluid Mech.* **13**, 427.

PHILLIPS, O. M. 1957 *J. Fluid Mech.* **2**, 417.

PHILLIPS, O. M. 1958*a* *J. Fluid Mech.* **4**, 426.

PHILLIPS, O. M. 1958*b* *J. Mar. Res.* **16**, 226.

PHILLIPS, O. M. 1958*c* Wave generation by a turbulent wind over a finite fetch. *Proc. 3rd U.S. Congr. Appl. Mech.* pp. 785–789.

PHILLIPS, O. M. 1961 *J. Geophys. Res.* **66**, 2889.

PHILLIPS, O. M. & KATZ, E. 1961 *J. Mar. Res.* **19**, 57.

PLATE, E. J. 1965 *La Houille Blanche* **6**, 595.

PLATE, E. J. & GOODWIN, C. 1965 The influence of wind on open channel flow. *Proc. of A.S.C.E. Conf. on Coastal Engr.*, Santa Barbara, California.

SCHLICHTING, H. 1960 *Boundary Layer Theory*, 4th ed. New York: McGraw-Hill.

THOMPSON, P. D. 1949 *Ann. N.Y. Acad. Sci.* **51**, 463.

WIEGEL, R. L. 1961 *Proc. 7th Conf. on Coastal Engr.* Council of Wave Research, Engr. Foundation, Berkeley, California.

URSELL, F. 1956 *Surveys in Mechanics.* Cambridge University Press.

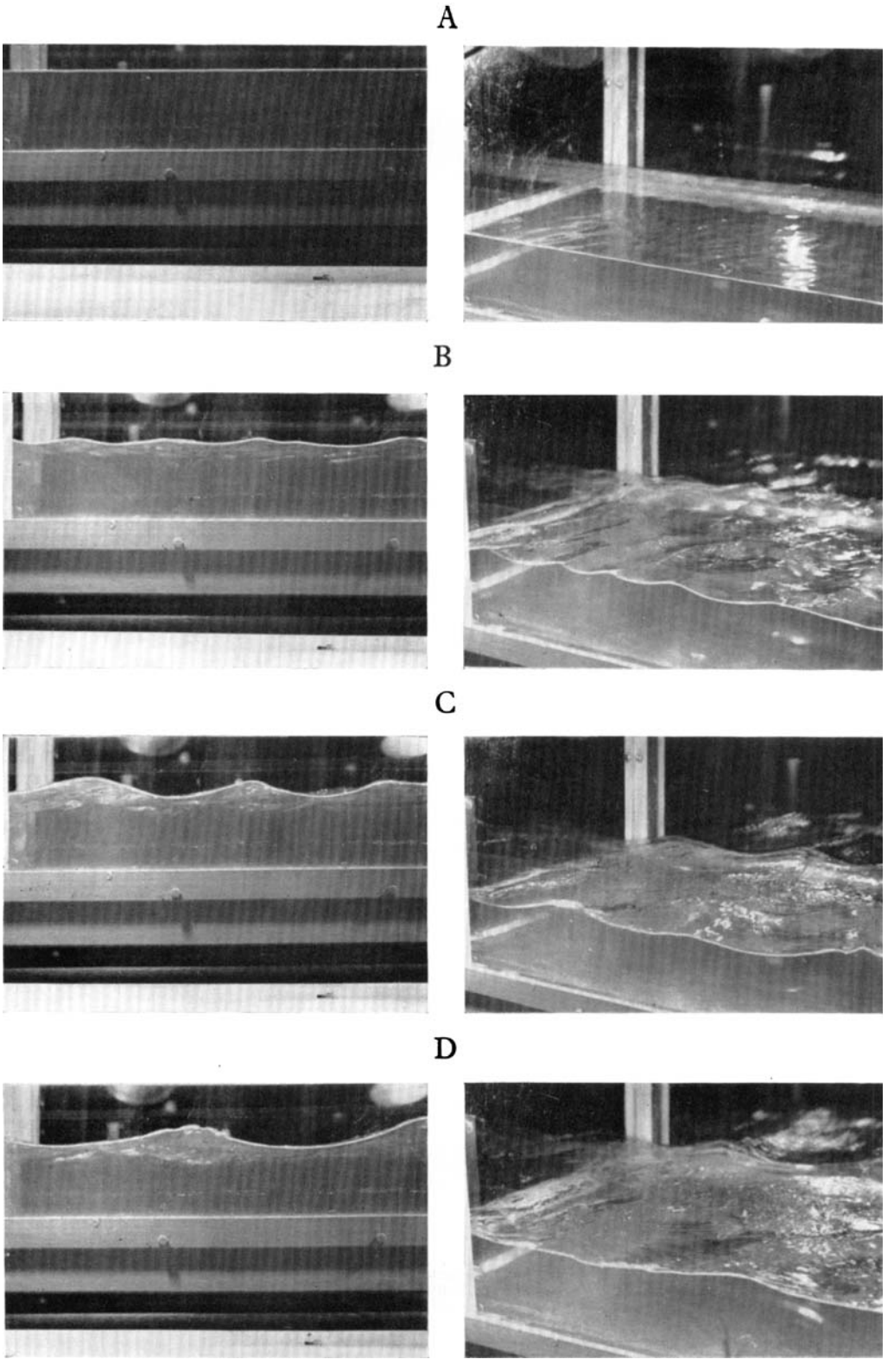

FIGURE 2. The development of wind waves on water 10·7 cm deep at a fetch of 8 m along the channel. A, $U_\infty = 4$ m/sec, $\overline{\lambda} = 3$ cm; B, $U_\infty = 6{\cdot}1$ m/sec, $\overline{\lambda} = 12$ cm; C, $U_\infty = 7{\cdot}6$ m/sec, $\overline{\lambda} = 15$ cm; D, $U_\infty = 9{\cdot}8$ m/sec, $\overline{\lambda} = 24$ cm.